PLOS PATHOGENS

RESEARCH ARTICLE

Vesicular trafficking permits evasion of cGAS/STING surveillance during initial human papillomavirus infection

Brittany L. Uhlorn[1☯], **Robert Jackson**[2☯], **Shuaizhi Li**[3], **Shauna M. Bratton**[4], **Koenraad Van Doorslaer**[1,2,3,5,6*], **Samuel K. Campos**[1,3,5,7*]

1 Cancer Biology Graduate Interdisciplinary Program, The University of Arizona, Tucson, Arizona, United States of America, **2** School of Animal & Comparative Biomedical Sciences, The University of Arizona, Tucson, Arizona, United States of America, **3** Department of Immunobiology, The University of Arizona, Tucson, Arizona, United States of America, **4** Department of Physiology, The University of Arizona, Tucson, Arizona, United States of America, **5** BIO5 Institute, The University of Arizona, Tucson, Arizona, United States of America, **6** Genetics Graduate Interdisciplinary Program, The University of Arizona, Tucson, Arizona, United States of America, **7** Department of Molecular & Cellular Biology, The University of Arizona, Tucson, Arizona, United States of America

☯ These authors contributed equally to this work.
* vandoorslaer@arizona.edu (KVD); skcampos@arizona.edu (SKC)

Citation: Uhlorn BL, Jackson R, Li S, Bratton SM, Van Doorslaer K, Campos SK (2020) Vesicular trafficking permits evasion of cGAS/STING surveillance during initial human papillomavirus infection. PLoS Pathog 16(11): e1009028. https://doi.org/10.1371/journal.ppat.1009028

Editor: Paul Francis Lambert, University of Wisconsin Madison School of Medicine and Public Health, UNITED STATES

Received: April 8, 2020

Accepted: October 2, 2020

Published: November 30, 2020

Data Availability Statement: All supplementary data files are freely available at https://github.com/KVDlab/Uhlorn-2020-evasion.

Funding: S.K.C. is supported by grant 1R01AI108751-01 from the National Institute of Allergy and Infectious Diseases, grant 1R01GM136853-01 from the National Institute of General Medical Sciences, and by a grant from the Sloan Scholars Mentoring Network of the Social Science Research Council with funds provided by

Abstract

Oncogenic human papillomaviruses (HPVs) replicate in differentiating epithelium, causing 5% of cancers worldwide. Like most other DNA viruses, HPV infection initiates after trafficking viral genome (vDNA) to host cell nuclei. Cells possess innate surveillance pathways to detect microbial components or physiological stresses often associated with microbial infections. One of these pathways, cGAS/STING, induces IRF3-dependent antiviral interferon (IFN) responses upon detection of cytosolic DNA. Virion-associated vDNA can activate cGAS/STING during initial viral entry and uncoating/trafficking, and thus cGAS/STING is an obstacle to many DNA viruses. HPV has a unique vesicular trafficking pathway compared to many other DNA viruses. As the capsid uncoats within acidic endosomal compartments, minor capsid protein L2 protrudes across vesicular membranes to facilitate transport of vDNA to the Golgi. L2/vDNA resides within the Golgi lumen until G2/M, whereupon vesicular L2/vDNA traffics along spindle microtubules, tethering to chromosomes to access daughter cell nuclei. L2/vDNA-containing vesicles likely remain intact until G1, following nuclear envelope reformation. We hypothesize that this unique vesicular trafficking protects HPV from cGAS/STING surveillance. Here, we investigate cGAS/STING responses to HPV infection. DNA transfection resulted in acute cGAS/STING activation and downstream IFN responses. In contrast, HPV infection elicited minimal cGAS/STING and IFN responses. To determine the role of vesicular trafficking in cGAS/STING evasion, we forced premature viral penetration of vesicular membranes with membrane-perturbing cationic lipids. Such treatment renders a non-infectious trafficking-defective mutant HPV infectious, yet susceptible to cGAS/STING detection. Overall, HPV evades cGAS/STING by its unique subcellular trafficking, a property that may contribute to establishment of infection.

the Alfred P. Sloan Foundation. K.V.D. is supported by State of Arizona Improving Health TRIF funds and by Institutional Research Grant number 128749-IRG-16-124-37-IRG from the American Cancer Society. B.L.U. is a graduate student supported by the National Science Foundation Graduate Research Fellowship Program, award DGE-1143953. CyVerse Discovery Environment (www.cyverse.org), is a computational infrastructure supported by the National Science Foundation under award numbers DBI-0735191, DBI-1265383, and DBI-1743442. The funders had no role in study design, data collection and analysis, decision to publish, or preparation of the manuscript.

Competing interests: The authors have declared that no competing interests exist.

Author summary

Persistent infection is the main risk factor for all HPV-associated cancers. However, cellular innate immune pathways exist to detect and limit viral infections. The cGAS/STING pathway senses cytosolic DNA to initiate antiviral IFN responses. Such responses would likely be detrimental towards the establishment of persistent HPV infections. We therefore hypothesize that HPV evades cGAS/STING detection via its unique vesicular trafficking mechanism. Here, we show that indeed HPV is a stealthy virus, capable of infecting keratinocytes with minimal activation of the cGAS/STING pathway. Such evasion is dependent on HPV's vesicular trafficking, as perturbation of vesicular integrity during infection results in sensing of virions.

Introduction

Human papillomaviruses (HPVs) are circular, double-stranded DNA viruses that infect and replicate in differentiating epithelium. HPV is the most commonly transmitted sexual infection, and oncogenic HPVs cause nearly 5% of all cancers worldwide and essentially all cervical cancers in women [1]. The HPV lifecycle and viral gene expression is dependent on differentiating epithelium [2–4]. To infect, HPV must traffic its circular dsDNA viral genome (vDNA) to the nucleus of basal keratinocytes, the only actively dividing cells within differentiating epithelium. Infected basal keratinocytes maintain vDNA episomes and serve as a reservoir for infected suprabasal cells that support the productive amplification of vDNA and assembly of progeny virions in upper epithelial layers [5,6]. Thus, persistently infected basal keratinocytes support sustained production of progeny virions to ensure efficient transmission within hosts. Notably, persistence of high risk HPV types is considered the risk factor for HPV-associated malignancies [7]. Unraveling the mechanisms that underlie HPV persistence is therefore important to understand both HPV lifecycle and cancer.

Structurally, HPV is a simple virus, yet it has evolved a unique mitosis-dependent mode of subcellular trafficking and delivery of vDNA to the host cell nucleus [8–10]. HPV virions bind to the extracellular matrix and cell surface heparan sulfate proteoglycans of basal keratinocytes, where upon proteolysis of the L1 and L2 capsid [11–13] and capsid conformational changes, the virion associates with entry receptor complexes and is endocytosed by the host cell [14–20]. As internalized virions travel through endosomal compartments, most of the L1 capsid is disassembled and degraded en route to the lysosome [9,21,22]. In complex with the vDNA, minor capsid protein L2 facilitates retrograde trafficking of the vesicular vDNA away from the degradative endo/lysosomal compartment to the lumen of the Golgi, where it resides during interphase [23–27]. L2 is an inducible transmembrane protein that can extend into the cytosol while remaining in complex with luminal vDNA by utilizing a transmembrane-like domain to protrude across local vesicular membranes to physically recruit retromer and other cytosolic sorting factors [8,28–32].

Upon entry into mitosis, vesicular L2/vDNA traffics away from the fragmenting Golgi and accumulates on metaphase chromosomes via a chromatin-binding domain within the central portion of L2 [33]. This L2-dependent chromosomal tethering of vDNA-containing vesicles ensures that the vDNA will be partitioned to the daughter cell nuclei after nuclear envelope reassembly and mitotic exit into G1. Our prior work using an L2-BirA fusion virus to report on L2/vDNA compartmentalization within vesicular membranes suggested that L2/vDNA may penetrate the Golgi-derived limiting membranes upon chromosome binding during

prometa/metaphase to fully translocate into the nuclear/cytosolic milieu of open mitosis [27,33]. However, work from the Sapp and Schiller laboratories suggests that L2/vDNA remains vesicular through the completion of mitosis [34,35]. Recent work also shows that some L1 pentamers retrograde traffic along with the L2/vDNA complex towards the nucleus, but their role is unclear [36,37]. Additional data suggests that some virions may even remain somewhat intact as partially disassembled capsids during Golgi and post-Golgi nuclear trafficking [34]. Within the daughter cell nuclei L2/vDNA somehow escapes the confines of these post-Golgi vesicles and recruits the nuclear ND10/PML body components necessary for efficient early viral gene expression [34,35,37,38].

Several other non-enveloped viruses, such as adenoviruses, nodaviruses, parvoviruses, picornaviruses, and reoviruses, have evolved more direct means of penetrating limiting membrane barriers for vDNA/vRNA delivery and subsequent infection of host cells [39–41]. The evolutionary rationale behind the unique mitosis-dependent vesicular trafficking mechanism of HPV is unknown. We and others speculate the trafficking mechanism may impart immunoevasive properties via vDNA shielding behind protective limiting membranes en route to the nucleus [8,34,42,43].

The innate immune system is adept at recognizing microbial nucleic acids as pathogen-associated molecular patterns (PAMPs) through a number of pattern recognition receptors (PRRs) [44]. Many PRRs also function to sense nucleic acids of cellular origin as danger-associated molecular patterns (DAMPs). These DAMPs typically consist of mislocalized or modified nucleic acids within the context of physiological stresses or cellular damage often associated with microbial infections [45,46]. In general, the activation of PRRs by nucleic acids leads to NFκB-dependent inflammatory cytokine responses and/or IRF3/7-dependent type-I interferon (IFN) antiviral responses.

The cGAS/STING pathway has emerged as a central innate immune sensing pathway for cytosolic DNA and downstream IFN responses [47–52]. Briefly, cytosolic DNA is recognized by the enzyme cGAS, triggering production of the cyclic dinucleotide 2',3'-cGAMP [53,54]. STING, a transmembrane endoplasmic reticulum (ER) protein [55], is activated upon binding to 2',3'-cGAMP [56]. Once activated by 2',3'-cGAMP, dimeric STING traffics to a perinuclear Golgi-like compartment [57,58], where it oligomerizes to recruit and activate TBK1 [59–61] to phosphorylate the transcription factor IRF3, stimulating an IFN response [55].

Initial entry, trafficking, and uncoating of many DNA viruses like herpesviruses (HSV-1, KSHV, HCMV), poxviruses (VACV, MVA), asfarviruses (ASFV), and adenoviruses (HAdV serotypes 2, 5, 7, and 35) have been shown to activate cGAS/STING [62–69]. Cellular sensing of initial HPV infection has not been formally investigated, but several studies have described roles for the early HPV oncogenes in antagonizing the cGAS/STING/IRF3 axis following establishment of infection [70–72]. Active antagonism of cGAS/STING by the early HPV proteins suggests that cGAS/STING responses would oppose persistent HPV infection. Indeed, IFN responses are detrimental to persistent HPV infections, reducing cellular proliferation and causing apoptosis, episome loss, mutation, and/or integration [73–77]. Likewise, it is well known that some HPV early genes–E5, E6, and E7 –counteract these detrimental antiviral IFN and IFN-stimulated gene (ISG) responses through a variety of mechanisms [78–81].

Given the ongoing interplay between HPV and antiviral responses, we postulate that evasion of cGAS/STING responses during initial infection would be beneficial to the viral life-cycle. We hypothesize that HPV's unique mitosis-dependent vesicular trafficking serves to enable such evasion. Here, we directly compare human keratinocyte cGAS/STING responses to HPV virion infection versus responses to cationic lipid transfection of dsDNA plasmid. We show a striking lack of IRF3 phosphorylation upon HPV infection. RNA-seq confirmed the lack of downstream antiviral IFN and ISG transcriptional responses to HPV infection.

Perturbance of intracellular vesicular membranes during infection results in antiviral responses to HPV infection, suggesting that HPV's distinctive vesicular trafficking underlies its stealthy abilities.

Results

HPV16 pseudovirus evades cGAS/STING responses during initial infection

We initially investigated cellular cGAS/STING responses to HPV16 pseudovirus (herein referred to as HPV) in HaCaT cells, spontaneously immortalized keratinocytes [82] that have a functional DNA-responsive cGAS/STING pathway [83–85]. HaCaT cells were either transfected with 250 ng of endotoxin free dsDNA plasmid (pGL3) for 90 min or infected with the HPV virion equivalent to 250 ng DNA (approximately equivalent to 950 ng L1 capsid, encapsidating pGL3 and non-specifically packaged cellular DNA). We wanted to ensure that cells were exposed to equivalent amounts of dsDNA during transfection and infection. Importantly, infection with increasing amounts of HPV results in a linear increase in luciferase activity (S1 Fig), suggesting that cells do not become saturated, thus allowing for the delivery of equivalent amounts of DNA by transfection and infection. H_2O or viral storage buffer (VSB) were used as controls for pGL3 or HPV in these experiments. Cellular responses to DNA transfection were followed over the next 12 hr by western blotting. Since HPV infection is slow and asynchronous [14] with different DNA delivery kinetics compared to transfection, HaCaT cells were infected with HPV and cGAS/STING activity was assessed over an extended 24 hr time course. In these experiments, virus was present until the sample was collected for analysis. An acute and robust IRF3 phosphorylation of serine 396 (pIRF3) was observed in response to DNA transfection (Fig 1A, left panel). In contrast, robust phosphorylation of IRF3 was not evident at any time point post-infection with HPV, indicating that the cGAS/STING pathway was not able to sense and respond to encapsidated vDNA (Fig 1A and 1B).

These HPV pseudovirions package pGL3, which contains a firefly luciferase expression cassette driven by an SV40 promoter. To gauge the relative pGL3 delivery between plasmid transfection and HPV infection, luciferase assays were performed 24 hr post-treatment. Since papillomaviruses lack specific genome packaging signals [86], HPV pseudoviruses generated in the 293TT system will package both pGL3 reporter plasmid and cellular dsDNA $\leq$ 8kb in size. The majority of virions will contain 293TT-derived DNA, with a smaller fraction containing pGL3 [87]. For simplicity, the encapsidated DNA will be referred to as "vDNA" herein, even though it is not the authentic viral genome. To account for partial packaging of pGL3 and host DNA, the luciferase numbers for the HPV16 infections were corrected by factoring in the measured virion:pGL3 ratio of 11.16 (See Materials and Methods). Despite a complete lack of pIRF3 responses, HPV infection resulted in equivalent luciferase activity compared to pGL3 transfected cells (Fig 1C), arguing that differences in cellular DNA delivery do not explain the apparent evasion of cGAS/STING surveillance by HPV.

While immortalized HaCaT cells represent a good model for the basal keratinocytes that HPV has tropism for *in vivo*, we sought to investigate cGAS/STING responses in cultured primary human foreskin keratinocytes (HFKs), a better model for the cells HPV naturally infects. Primary HFKs were transfected with 500 ng pGL3 or infected with the viral DNA equivalent. As with HaCaT cells, transfection of cells with H_2O or addition of VSB to cells were used as controls. pGL3 transfection resulted in robust activation of the cGAS/STING pathway, as seen by the detection of phosphorylated STING (pSTING) and pIRF3 (Fig 2). As before, HPV infection did not activate the pathway as detected by phosphorylation of STING or IRF3 during infection (Fig 2A). We observed a delay in activation between HaCaTs (peak near 90 min) and HFKs (4 hr). This may be due to differences in transfection efficiency between primary HFKs

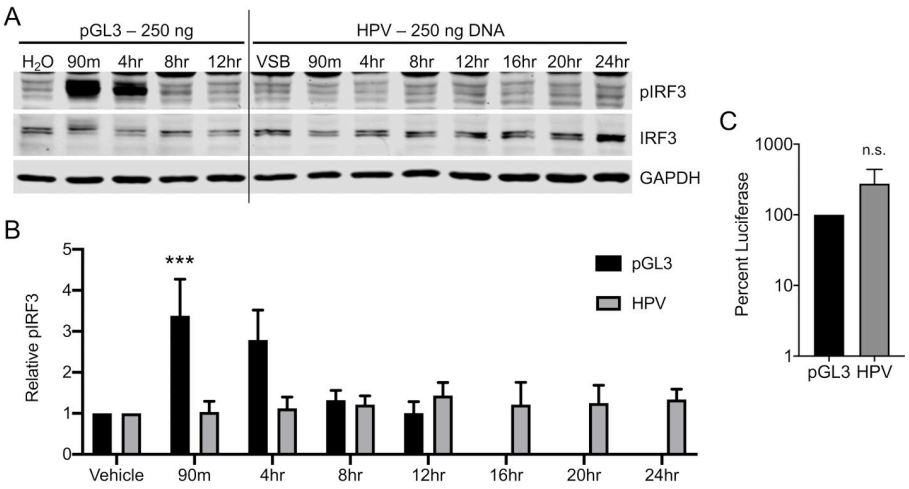

Fig 1. HPV16 evades cGAS/STING responses in HaCaTs during initial infection. cGAS/STING responses to pGL3 and HPV PsV in HaCaTs. **(A, B)** Cells were either transfected for 90 min with 250 ng pGL3 or infected for the duration of the experiment with 950 ng L1 (equivalent to 250 ng DNA) of HPV16 virions. Cells were harvested at various times post-treatment and cGAS/STING responses assessed via western blotting. **(A)** IRF3 was phosphorylated, most prominently at 90 min and 4 hr post pGL3 transfection, while IRF3 was not phosphorylated at any time post HPV16 infection, representative blot of $n = 4$ biological replicates. **(B)** Densitometric quantification of western blots, $n = 4$ biological replicates. Statistics calculated by two-way ANOVA ($P_{interaction} = 0.0138$) followed by Sidak's multiple comparison test ($^{***}P < 0.005$). **(C)** Cells were either transfected for 90 min with 250 ng pGL3 or infected for the duration of the experiment with an equivalent amount of HPV virions. Luciferase activity was measured 24 hr post-treatment, normalized to GAPDH, and corrected for pGL3 encapsidation as described in *Materials and Methods*. Differences were not significant (n.s.) by unpaired *t*-test, $n = 3$ biological replicates.

https://doi.org/10.1371/journal.ppat.1009028.g001

and HaCaTs, or the kinetics of cellular activation may be slower in primary cells. To ensure comparable delivery of the 500 ng dsDNA via HPV virions compared to plasmid transfection we performed a luciferase assay 24 hr post-transfection/infection. As with HaCaT cells, HPV

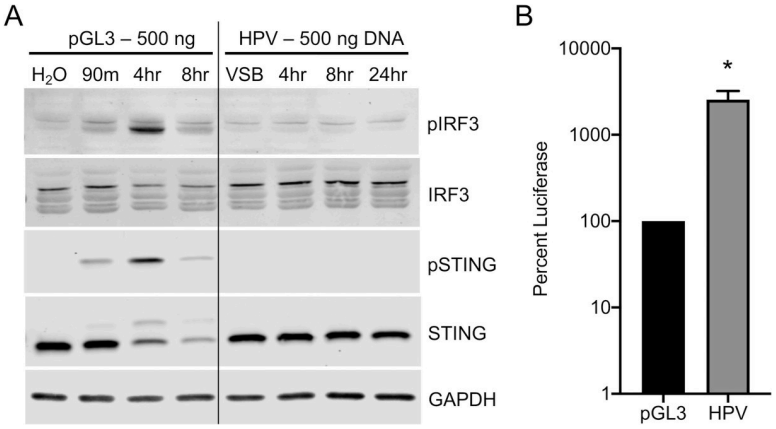

Fig 2. HPV16 evades cGAS/STING responses in HFKs during initial infection. cGAS/STING responses to pGL3 and wildtype HPV in primary HFKs. **(A)** HFKs were either transfected for 90 min with 500 ng pGL3 or infected for the duration of the experiment with 1900 ng L1 (equivalent to 500 ng DNA) of HPV virions. Cells were harvested at various times post-treatment and cGAS/STING responses assessed via western blotting. **(A)** IRF3 was phosphorylated 4 hr post pGL3 transfection, while IRF3 was not phosphorylated at any time post HPV infection with HPV PsV. representative blot of $n = 3$ biological replicates. **(B)** Cells were either transfected for 90 min with 250 ng pGL3 or infected for the duration of the experiment with an equivalent amount of HPV virions. Luciferase activity was measured 24 hr post-treatment, normalized to GAPDH, and corrected for pGL3 encapsidation as described in *Materials and Methods*. $^{*}P < 0.05$ by unpaired *t*-test, $n = 3$ biological replicates.

https://doi.org/10.1371/journal.ppat.1009028.g002

infection again yielded robust luciferase activity as compared to plasmid transfection of HFKs (Fig 2B). These data further support a stealthy mode of HPV infection whereby cGAS/STING responses are avoided, despite effective delivery of encapsidated pGL3 DNA.

Transcriptional responses to DNA transfection and HPV16 infection of primary HFKs

We performed RNA-seq analysis to profile cellular transcriptional responses to dsDNA delivered via cationic liposomes or HPV pseudovirions (Fig 3, S1 Data, S2 Data). As above, HFKs were either transfected with 500 ng pGL3 or infected with the 500 ng DNA equivalent of HPV virions. Total RNA was extracted at the indicated timepoints. At 4 hr post-transfection, 142 genes (95 up and 47 down) were differentially expressed (Fig 3A, S3 Data) in HFKs relative to mock (H_2O complexed with transfection reagent) transfection ($n = 2$, P-adj < 0.05). The up-regulated genes (Fig 3B), representing expected transcriptional responses to cytosolic DNA, were functionally enriched (see S4 Data for detailed results) for 82 Gene Ontology (GO) Biological Processes, including "defense response to virus" (GO:0051607, P-adj = 2.26 x 10^{-15}) as the top hit among innate immune-related terms. Of the 10 enriched Reactome Pathways, the

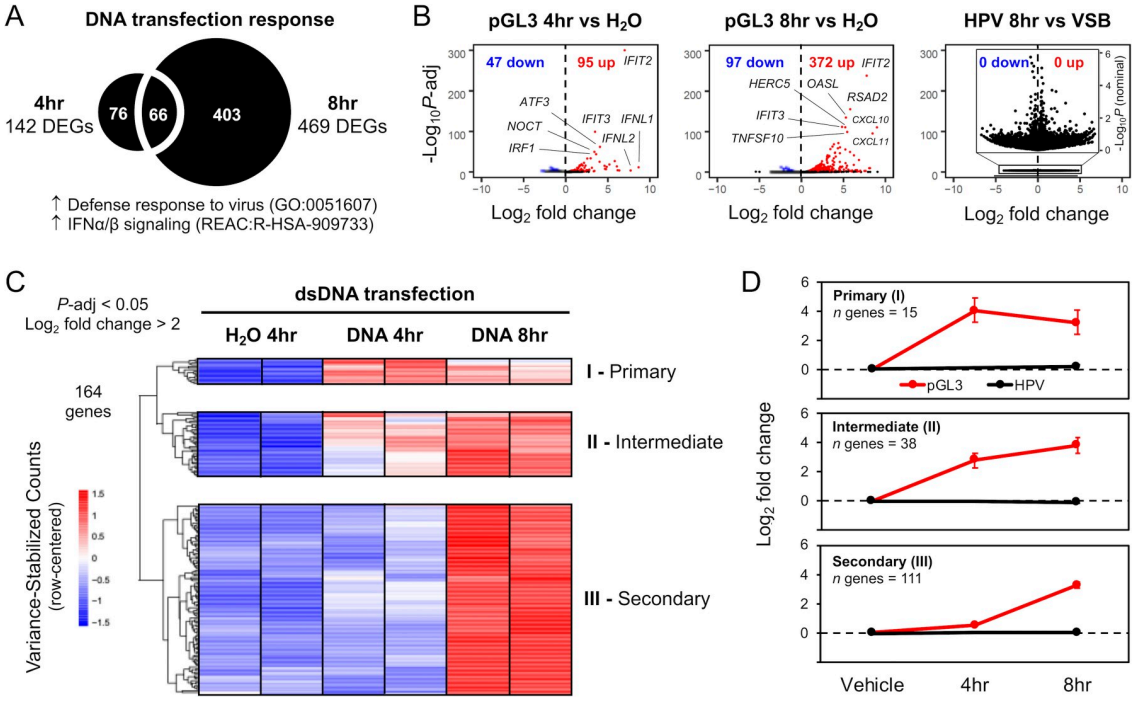

Fig 3. HPV16 virion infection does not activate cellular responses to dsDNA. RNA-seq was used to transcriptionally profile cellular responses to pGL3 DNA introduced via liposome transfection or HPV virion infection. **(A)** Relative to H_2O mock-transfection, there were 142 significantly (P-adj < 0.05) differentially expressed genes (DEGs) at 4hr and 469 DEGs at 8hr post-transfection, with up-regulated genes functionally enriched for biological processes and pathways related to defense responses to virus and IFN signaling. **(B)** Volcano plots for 4 and 8hr pGL3 transfections ($n = 2$) show significantly DEGs (P-adj < 0.05), with up-regulated genes (red) related to strong innate immune signaling responses. No response was activated 8hr following HPV virion infection ($n = 3$) relative to viral storage buffer (VSB); inset volcano plot is re-scaled, using nominal (unadjusted) P-values, to show distribution of genes that do not reach significance. **(C)** Heatmap of variance-stabilized counts, row-centered, for the top up-regulated cellular response genes (P-adj < 0.05, $\log_2$ fold change > 2, for 4 and 8hr pGL3-transfection: 164 genes). Genes clustered into three main groups, corresponding to temporal responsiveness post-transfection: cluster I (immediate/primary response at 4hr), cluster II (intermediate response at 4 and increasing at 8 hr), and cluster III (secondary response at 8 hr). **(D)** Metagene $\log_2$ fold change values were computed by aggregating response data of all genes within each cluster. Error bars represent 95% confidence intervals for each gene cluster.

https://doi.org/10.1371/journal.ppat.1009028.g003

top hit was "Interferon alpha/beta signaling" (REAC:R-HSA-909733, *P*-adj = 1.16 x 10^{-7}). In line with our western blot data (Figs 1 and 2), IRF3 was the top transcription factor signature related to these up-regulated genes (*P*-adj = 8.61 x 10^{-10}). The top five most significantly up-regulated genes at 4 hr post-transfection included *IFIT2*, *IFIT3*, *ATF3*, *NOCT*, and *IRF1*; the genes with the highest fold change, ranging from ~70 to 400 times above baseline, were *IFNL1*, *IFNL2*, *IFIT2*, *NEURL3*, and *ZBTB32*.

At 8 hr post-transfection, 469 genes (372 up and 97 down) were differentially expressed (Fig 3A, S3 Data) in HFKs ($n = 2$, *P*-adj < 0.05). These up-regulated genes were also functionally enriched for IFN signaling, with the top five most significantly up-regulated genes (Fig 3B) at 8 hr post-transfection including *IFIT2*, *RSAD2*, *OASL*, *IFIT3*, and *HERC5*. The genes with the highest fold change at 8 hr, ranging from ~200 to 500 times above baseline, were *CXCL10*, *CXCL11*, *IFNL1*, *GBP4*, and *IFIT2*. Investigation of the heatmap (Fig 3C) identifies 3 main functional groups of genes (Fig 3D). Genes that are upregulated acutely, at 4 hr (I; 'Immediate'/'Primary'), and either go back down ('Immediate') or remain up at 8 hr ('Primary'), genes that are upregulated by 4 hr and continue to increase throughout the experiment (II; 'Intermediate'), and a group of genes that are upregulated by 8 hr but were not significantly affected at the 4 hr timepoint (III; 'Secondary'). Complete gene sets for each cluster are provided in supplementary S5 Data.

While 500 ng of pGL3 delivered via cationic liposomes triggered a robust IRF3-based transcriptional response in HFKs, with the strongest overall response at 8 hr post-transfection, the equivalent amount of DNA delivered via HPV pseudovirus infection yielded no response (Fig 3B, right panel). At 8 hr post-infection, there were no genes differentially expressed in HFKs relative to mock infection with VSB ($n = 3$). Importantly, preliminary analysis of the later 24 hr time-point did not show activation of IFN or ISG related transcription compared to VSB treatment (S2 Fig). Overall, compared to tranfection, HPV infection is unable to induce a classic innate immune response signature in primary HFKs (Fig 3B and 3D).

Fig 4 highlights the transcriptional response of different IFN and ISGs that were previously demonstrated to interact with the HPV lifecycle (see Discussion). These responses fall into the same functional classes identified in Fig 3: 1) an acute response peaking at 4 hr (e.g., *IFNB1*, *IFNL1*, *IFNL2*, *ATF3*, and *IRF1*), 2) an intermediate response with an apparent peak at 8h (e.g., IFIT1, HERC5, IRF7, ISG15, and *CDKN2C*), and 3) genes belonging to class III, displaying a 'secondary' response (e.g., *TNFSF10*, *RSAD2*, *IFI16*, *CXCL10*, and *CXCL11*). Similar to Fig 3, there is no evidence (Fig 4) that HPV infection upregulates the transcription of these genes.

Bypassing HPV's natural trafficking pathway activates cGAS/STING

cGAS/STING is capable of sensing the incoming vDNA from a number of viruses including adenoviruses, poxviruses, herpesviruses, and the reverse-transcribed cDNA products of lentiviruses like HIV [62,63,88,89]. These viruses either breach (non-enveloped viruses) or fuse with (enveloped viruses) intracellular limiting membranes to provide vDNA-capsid complexes access to the cytosol and eventually reach the nucleus, or remain in the cytoplasm in the case of pox. In contrast, HPV uses the minor capsid protein L2 to transport vDNA within vesicular membranes en route to the nucleus during mitosis-dependent subcellular trafficking [8–10]. We hypothesize this unique vesicular trafficking enables evasion of cellular cGAS/STING surveillance.

To test this hypothesis, we stimulated premature membrane penetration of HPV vDNA to determine if cGAS/STING would then be capable of detecting HPV infection. As no HPV capsid protein mutations are known to cause leakage or transfer of vDNA across vesicular

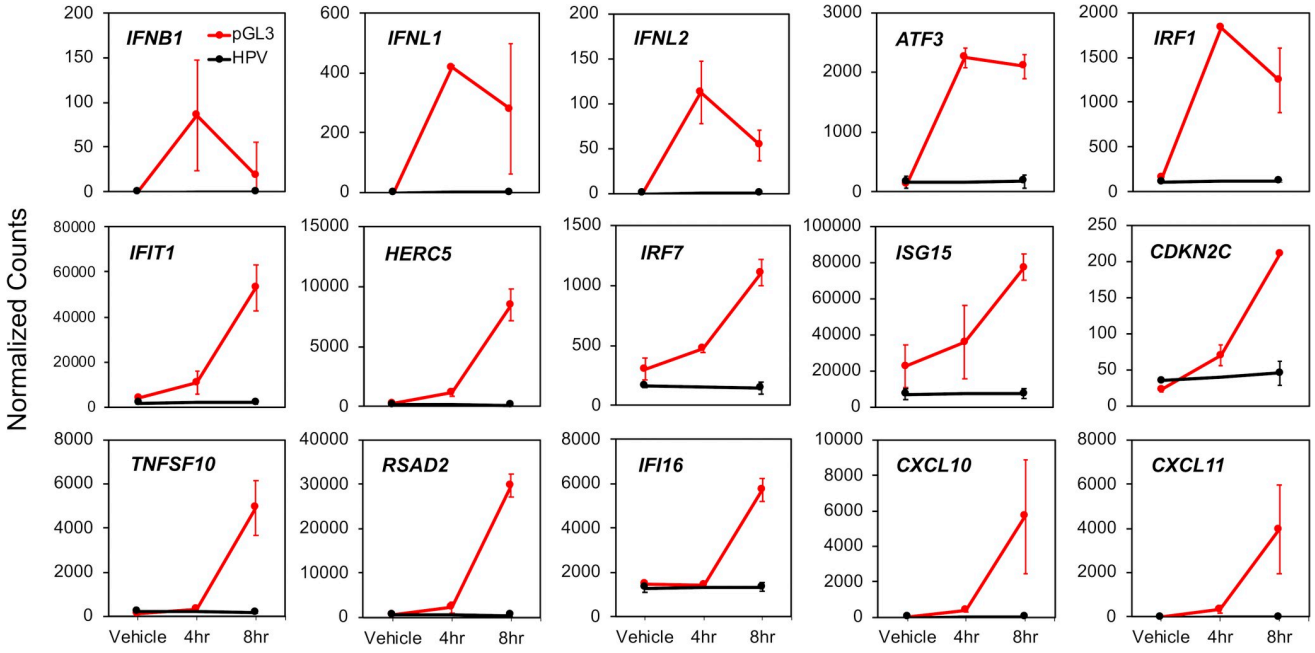

Fig 4. HPV-related DNA-responsive cellular genes are not induced by virion infection. Normalized RNA-seq count data were plotted for a subset of 15 DNA-responsive cellular genes selected based on prior literature indicating a relationship with HPV. Error bars represent 95% confidence intervals ($n = 2$ for pGL3 transfection, red, and $n = 3$ for HPV virion infection, black).

https://doi.org/10.1371/journal.ppat.1009028.g004

membranes, we instead used cationic lipids which are known to perturb intracellular limiting membranes [90–92]. Indeed, our prior work using a sensitive enzyme-based L2 membrane penetration assay showed that even low amounts of cationic lipid (Lipofectamine RNAiMax) during HPV infection are capable of disrupting vesicular membranes that normally limit HPV from cytosolic exposure (see supplemental figure S2 in ref [27]).

HPV pseudovirions encapsidating pGL3 were mixed to the cationic lipid Lipofectamine 2000, as described in *Materials and Methods*. Transmission electron microscopy of this mixture revealed that intact HPV16 virions were in the close vicinity of submicron cationic lipid complexes (Fig 5A). We next assessed the ability of wildtype HPV (wildtype L2 protein) and the post-Golgi trafficking defective L2 R302/5A mutant HPV to deliver vDNA to the nucleus in the presence of cationic lipids compared to control media. The R302/5A mutation in L2 renders particles non-infectious (Fig 5B). Particles that contain R302/5A mutant L2 undergo normal early trafficking but fail to penetrate Golgi-derived vesicular compartments due to defective binding between the mutant L2 and host mitotic chromosomes [27,33,93]. R302/5A vDNA therefore remains cloaked within vesicular membranes, failing to reach the nucleus. Addition of cationic lipids caused a ~60% decrease in wildtype HPV infectivity, as measured by luciferase assay for the delivery of virion-packaged pGL3 to the nucleus (Fig 5B). In stark contrast, cationic lipids rescued the infectivity of R302/5A mutant virus to levels comparable to that of wildtype HPV in the presence of cationic lipids (Fig 5B). The natural subcellular retrograde trafficking of vDNA is dependent on endosomal acidification, furin cleavage of L2, and γ-secretase activity. Small molecule compounds that perturb these processes are potent inhibitors of HPV16 infection [8]. The cationic lipid-dependent infectivity of R302/5A was insensitive to endosomal acidification inhibitor BafA, furin inhibitor dRVKR, or γ-secretase inhibitor XXI (Fig 5C). Interestingly, the HPV16-specific monoclonal antibody H16.V5 but not the BPV1-specific B1.A1 was able to completely neutralize cationic lipid-dependent

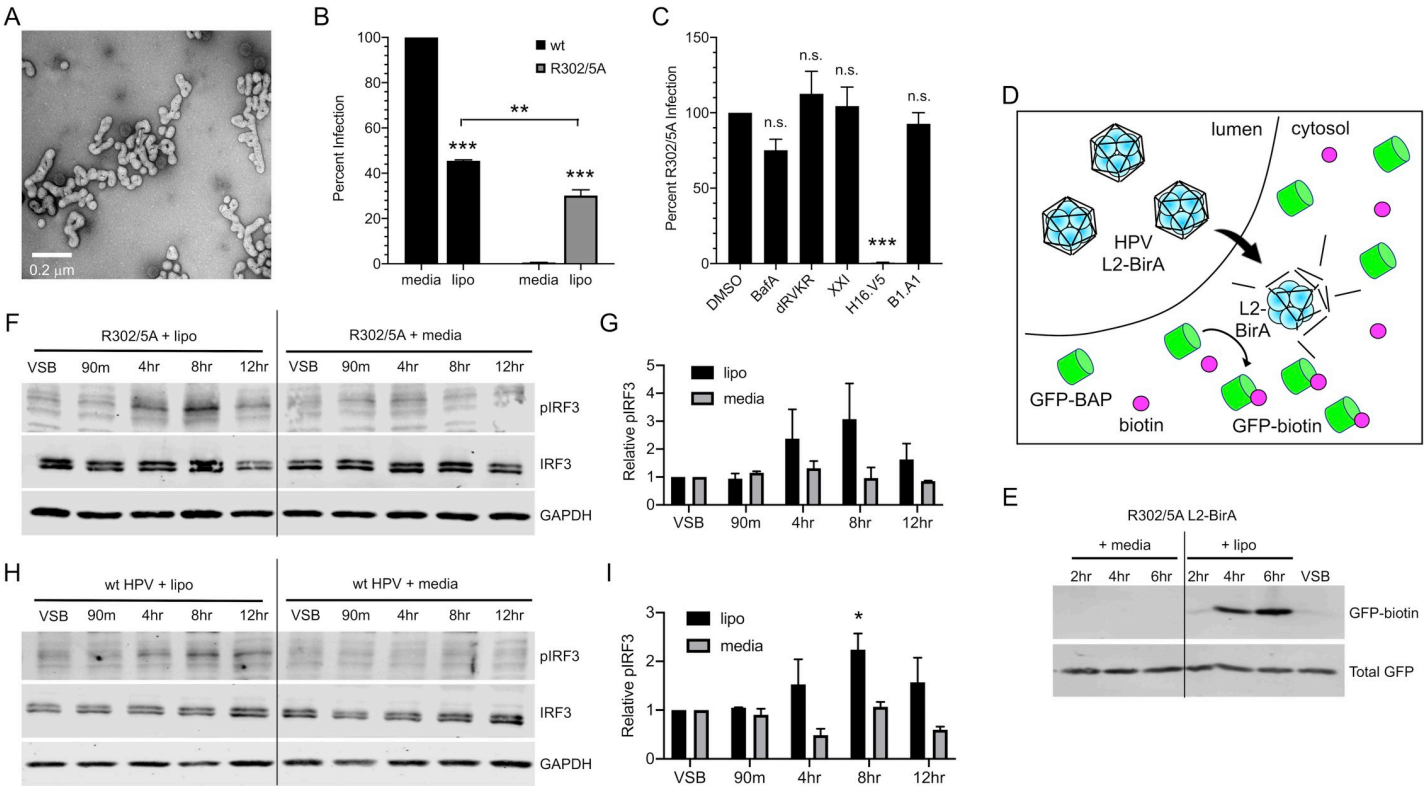

Fig 5. Bypassing HPV's natural trafficking pathway activates cGAS/STING. Addition of cationic lipids during infection with translocation-deficient R302/5A mutant HPV restores infectivity and allows for cGAS/STING sensing. **(A)** Electron micrograph of HPV complexed with the cationic lipid Lipofectamine 2000. **(B)** HaCaTs were infected with 2e8 vge/well of wildtype (capsid) or R302/5A virion +/- cationic lipid (lipo) for 4 hr and infection was measured by luciferase assay 24 hr post-infection. While naturally non-infectious, addition of cationic lipids restored infectivity of the R302/5A mutant to levels nearly comparable to those of wildtype HPV. Statistics calculated by one-way ANOVA ($P < 0.001$) followed by Tukey's multiple comparisons test ($^{**}P < 0.01$, $^{***}P < 0.005$), $n = 3$ biological replicates **(C)** R302/5A infection in the presence of cationic lipids is insensitive to biochemical inhibitors of endosomal acidification (BafA), furin (dRVKR), γ-secretase (XXI), and BPV1-specific Nab B1.A1, but is sensitive to HPV16-specific H16.V5. With exception of H16.V5 ($^{***}P < 0.005$), differences were not significant by one-way ANOVA followed by Dunnett's multiple comparisons test, $n = 3$ biological replicates. **(D)** Schematic of the membrane penetration assay using L2-BirA viruses in HaCaT cells stably expressing cytosolic GFP-BAP. Conditions enabling early membrane penetration result in L2-BirA dependent generation of GFP-biotin. **(E)** Membrane penetration assay. R302/5A L2-BirA virions (250 ng L1) were complexed +/-lipo or media as described. HaCaT-GFP-BAP cells were infected with virus/complexes for the indicated times prior to detection of GFP-biotin and total GFP by SDS-PAGE and western blot. **(F-I)** Cells were infected for 4 hr with R302/5A **(F, G)** or wildtype HPV16 **(H, I)** virion equivalent of 250 ng DNA +/- cationic lipids (lipo) as described in *Materials and Methods*. Addition of cationic lipids during virus infection resulted in IRF3 phosphorylation at 4 hr and 8 hr, while virus infection in media alone did not induce IRF3 phosphorylation, representative blots shown of $n = 2$ biological replicates in both **(F, H)**. **(G, I)** Densitometric quantification of western blots. **(G)** Statistics were calculated by two-way ANOVA followed by Dunnett's multiple comparisons test. Due to technical aspects of background variability and few replicates, differences did not reach statistical significance ($P_{interaction} = 0.331$, $P = 0.125$ at 8 hr time point), $n = 2$ biological replicates. **(I)** Statistics were calculated by two-way ANOVA ($P_{interaction} = 0.1359$), followed by Dunnett's multiple comparisons test ($^{*}P < 0.05$), $n = 2$ biological replicates.

https://doi.org/10.1371/journal.ppat.1009028.g005

infection of R302/5A. Collectively, these data indicate that although initial entry of intact particles into the endosomal compartment is still L1-mediated, cationic lipids mediate vesicular escape of HPV16 to rescue infectivity of R302/5A via an alternative route, independent of the classical HPV16 vesicular trafficking pathway.

Next we utilized our previously published L2-BirA system [27,94] to assess membrane penetration of virions in the presence of cationic lipids. This system works based on fusion of the biotin protein ligase BirA to the L2 capsid protein. BirA catalyses covalent addition of biotin to proteins tagged with a small peptide substrate- the "biotin acceptor peptide" (BAP). The system works as a compartmentalization assay to detect virus reaching the cytosol. Vesicular membranes prevent lumenal L2-BirA virus from contacting the cytosolic GFP-BAP substrate until the virus penetrates or crosses limiting vesicular membranes. Once the L2-BirA virus

penetrates, the BirA will be in contact with GFP-BAP substrate and GFP-biotin can be detected (Fig 5D). Our prior work showed that R302/5A mutant L2-BirA viruses were incapable of penetrating limiting membranes in this system due to the mutations in L2 [27]. Furthermore, penetration by wt L2-BirA virus is mitosis-dependent, and occurs only after proper Golgi trafficking and progression of cells through G2/M. Therefore, in a bulk infection of an asynchronous cell population, the earliest time GFP-biotin can be detected is 8-10 hr post infection [27].

We performed a brief timecourse infection with R302/5A mutant L2-BirA viruses, complexed with or without cationic lipid Lipofectamine 2000 as described above. Infection with R302/5A L2-BirA failed to generate any GFP-biotin within the first 6 hr, as expected. In contrast, the presence of Lipofectamine 2000 resulted in robust GFP-biotin signal by 4 hr and 6 hr (Fig 5E), indicative of premature membrane penetration caused by the cationic lipid Lipofectamine 2000.

Since the use of cationic lipids to bypass the natural subcellular trafficking pathway of HPV rescued infectivity of R302/5A mutant virions by perturbing intracellular membranes, we examined whether premature disruption of vesicular membranes by cationic lipids would allow for activation of the cGAS/STING pathway by HPV16. HaCaT cells were infected with R302/5A virions +/- cationic lipids and cGAS/STING activity was assessed by pIRF3 blot as before. Similar to wildtype HPV infection (Fig 1), R302/5A mutant infection alone did not activate the cGAS/STING pathway. However, premature vesicle disruption allowed for robust sensing of DNA delivered by R302/5A infection as measured by IRF3 phosphorylation, most prominently at 4 hr and 8 hr post-infection (Fig 5F and 5G). Similar results were seen in experiments using wt HPV16 particles (Fig 5H and 5I). These results indicate that when cationic lipids allow HPV16 virions to breach vesicular compartments, the cGAS/STING pathway is activated, generating a pIRF3 response.

Discussion

Cells are equipped with numerous PAMP- and DAMP-sensing PRRs, designed to detect the first signs of cellular stress and respond in an IRF3 and NFκB transcription factor-dependent manner to induce the expression of IFN, antimicrobial ISGs, and proinflammatory cytokine genes [95]. Geared towards recognizing dsDNA in the cytoplasm of a cell, the recently characterized cGAS/STING pathway has proven to be a critical arm of innate immunity and an important cellular antiviral defense system that is targeted for evasion and/or antagonism by many different viruses [51,52,96].

The HPV early proteins have been shown to block cGAS/STING and downstream IRF3-dependent IFN responses, as well as NFκB-dependent cytokine responses through a variety of mechanisms [70,71,79–81,97,98]. The early viral proteins that counteract the cellular antiviral responses are not packaged within incoming virions. Thus, passive evasion mechanisms to limit early detection by the innate immune system during early infection would likely benefit later stages of the viral lifecycle. Viral blunting of these cell intrinsic and extrinsic responses likely promotes viral persistence by enabling maintenance of episomal vDNA and reducing inflammatory responses that cause activation of antigen-presenting cells and promote adaptive antiviral immune responses [99].

Here we investigate cGAS/STING responses to initial HPV infection. Although some prior work has reported minimal induction of IFN and downstream ISGs in response to HPV and canine PV infection [100,101], no studies have directly addressed cGAS/STING responses to incoming HPV virions. Importantly, other than the viral L1 and L2 proteins that are part of the incoming viral capsid, the pGL3 reporter plasmid does not express any papillomavirus

proteins. We find that while keratinocytes mount acute pIRF3 and downstream IFN/ISG responses to dsDNA plasmid transfection, dsDNA delivered through HPV infection proceeds undetected by cGAS/STING. To allow for direct comparison, we infected cells with the virion equivalent of 500 ng DNA, corresponding to a multiplicity of infection (MOI) of 400,000 virions/cell. These super-physiological conditions strengthen the hypothesis that a physiological infection is unlikely to be detected. The transcriptional response to dsDNA included type-I *IFNB1*, type-III *IFNL1* and *IFNL2*, and many IFN-dependent ISGs and chemokines (Figs 3 and 4). Many of these ISGs, like *IFIT1/2/3*, *ISG15* and *CXCL10/11*, can be upregulated directly through IRF3-mediated transcription, in addition to secondary IFN-dependent signaling (pSTAT1/pSTAT2/IRF9) mechanisms in certain cellular contexts [102–104].

Not surprisingly, many of these proteins have been implicated in the viral lifecycle. *IFIT1* (p56/ISG56) has the potential to directly restrict persistent HPV infection via inhibition of E1-dependent episomal vDNA maintenance [77]. *ISG15* encodes a ubiquitin-like molecule with broad antiviral activity. *HERC5* is an E3 ligase that catalyzes the addition of ISG15 to nascent viral proteins leading to the restriction of HPV replication [105]. CXCL10, CXCL11, and related CXCL-family chemokines attract activated T cells via CXCR3 [106,107]. These chemokine responses may also be detrimental to HPV persistence, as evidenced by a recent mouse papillomavirus study where MmuPV1 was observed to specifically downregulate stress keratin-induced expression of CXCR3 ligands including CXCL10 [108]. *IFI16* is a DNA-binding inflammasome component and can restrict HPV replication by epigenetically silencing viral gene expression reducing vDNA copy number [109,110]. Several of the genes upregulated by dsDNA transfection are counteracted by papillomavirus gene products. *IRF1* and *IRF7* gene products augment IFN/ISG responses. IRF1 activity is counteracted by the E7 protein from high risk HPVs [111,112]. Similarly, *RSAD2* (viperin) has broad antiviral activity and is downregulated by cutaneous HPV2 E7 [113].

Double-stranded DNA transfection also induced cell survival and proliferation modulators like *ATF3*, *CDKN2C*, and *TNFSF10*. *ATF3* interferes with E6's ability to degrade p53 by preventing E6AP from binding to p53, thus interfering with HPV immortalization [114]. Interestingly, *ATF3* expression is downregulated in cervical cancer [114]. *CDKN2C* encodes p18INK4C, which restricts cellular proliferation through inhibition of CDK4 and CDK6 [115]. Expression of *CDKN2C* is upregulated by oncogenic E6 proteins [116], suggesting that the virus must be able to replicate in the presence of this anti-proliferative signal. *TNFSF10* encodes TRAIL, a member of the TNF family of ligands that can initiate apoptosis [117]. The viral E5 protein counteracts TRAIL signaling to block apoptosis and promote HPV infection [118,119]. If activated, the induction of cellular effectors would likely restrict initial HPV replication following infection. Thus, initial evasion of cGAS/STING and these downstream cellular IRF3/IFN/ISG responses would likely be beneficial to long-term HPV infection. Collectively, our data suggest that the ability of the viral proteins to antagonize so many of these effectors is not to counteract sensing of the viral DNA upon initial infection. Rather, counteraction of these antiviral/antitumor responses is important for later steps in the viral lifecycle.

Interestingly, HPV16 infection is sensed when vesicular membranes are perturbed by the inclusion of cationic lipids during infection. These findings also indicate that the chromatinized encapsidated vDNA is insufficient to (completely) mask the viral genome from cGAS surveillance, as recent reports have shown that the nucleosomal components of mitotic chromatin prevents efficient cGAS activation by dsDNA [85,120,121]. We conclude that HPV's unique L2-dependent vesicular membrane trafficking effectively shields the vDNA PAMP from cytosolic cGAS/STING surveillance during nuclear transit, likely contributing towards viral persistence. A recent report describes a DNA-PK mediated DNA-sensing mechanism

that appears to be specific to linear DNA [122]. Since the HPV genome is circular, it is unlikely that this pathway would be involved in the sensing of HPV infection. Furthermore, during production, HPV pseudovirus particles package linear 293TT DNA. During infection with wildtype L2 virions, we did not detect activation of STING of IRF3, suggesting that linear DNA is also shielded.

Our data suggest that papillomaviruses use subcellular trafficking to evade innate immune detection. Variation in subcellular trafficking routes has been shown to influence innate immune responses to other viruses. Different trafficking mechanisms during HAdV entry of several cell types have been shown to affect the stimulation of certain PRRs, influencing distinct immune responses that are dependent on particular virus- and cell-type combinations [123]. For example, different HAdV serotypes naturally vary in their receptor usage as well as downstream early vs. late endosomal trafficking pathways. These inherent differences in HAdV serotypes have been shown to affect innate TLR-dependent sensing of the virus [124]. For example, dynamin-2 (DNM2) is a cellular GTPase involved in microtubule-dependent transport and scission of endosomes. Modulation of DNM2 affects the trafficking of HAdV, resulting in an altered cellular cytokine response to infection [125]. Reovirus T1D and T3L strains elicit differing magnitudes of IRF3-dependent IFN responses in a manner dependent on viral uncoating during the late steps of viral entry and trafficking [126]. In the case of HIV, the CD4 receptor and the cellular dynein adapter BICD2 play roles in viral trafficking, influencing innate sensing and downstream IFN/ISG responses in infected cells [127,128]. Likewise, host phospholipase D affects innate sensing of the influenza A virus by modulation of entry [129].

Thus, while differing modes of trafficking can affect cellular responses to many viruses, HPV appears to have evolved an extremely covert means of evading cellular IRF3-dependent responses by hiding incoming vDNA inside the vesicular trafficking network. Other viruses may have evolved similar trafficking-dependent immunoevasion strategies. Adeno-associated viruses (AAVs) are parvoviruses that have recently been shown to retrograde traffic to the Golgi [130]. Although cellular pIRF3 responses to initial infection have yet to be investigated, it is tempting to speculate that they too may hide the genome from cytoplasmic DNA sensors. The polyomaviruses (PyVs) are dsDNA viruses that are structurally similar to papillomaviruses. PyVs also undergo subcellular retrograde transport after cellular uptake, but unlike HPVs, SV40 and the related BKPyV and JCPyV bypass the Golgi and traffic directly from endosomes to the ER, where redox-dependent chaperones loosen the VP1 capsid to expose membrane-interacting minor capsid proteins VP2/3 [131–133]. The post-ER fate of the PyV vDNA is unclear, with data suggesting cell- and virus-type specific differences in transport of vDNA from ER to cytosol/nucleus [134]. A recent study found a striking lack of pIRF3 and downstream IFN/ISG responses to BKPyV infection [135], similar to what we observe with papillomaviruses in the present manuscript.

Of note, these smaller viruses do not package tegument or core proteins that may be able to counteract cytoplasmic sensors or their downstream effector proteins. Indeed, these viruses, like papillomaviruses, need to avoid triggering these cytoplasmic sensors. This raises the possibility that multiple viral families may have converged on a trafficking-dependent immunoevasive strategy.

Materials and methods

Tissue culture

HaCaT cells [82] and HaCaT-GFP-BAP cells that stably express cytosolic GFP-BAP [27] were grown in high glucose DMEM supplemented with 10% FBS and Ab/Am. An additional 200

ng/mL puromycin (EMD Millipore 508838) was used for maintaining stable expression in HaCaT-GFP-BAP cells. Cells were maintained at 37˚C with 5% CO_2 and passaged every 2–3 days. Murine J2 fibroblasts were grown in high glucose DMEM supplemented with 10% NCS, 1% penicillin/streptomycin and 1% L-glutamine. Cells were maintained at 37˚C with 5% CO_2 and passaged every 3–4 days. To create a feeder layer to support the growth of primary human foreskin keratinocytes, J2 fibroblasts were irradiated every 3–4 days. Cells were removed from continuing culture flasks, resuspended in media in a 15 mL conical, and irradiated with 6000 rads using a Gammacell 40 cesium-137 source as described [136]. Irradiated cells were plated at 1 million cells per 10 cm plate to later be used for support of primary keratinocytes. Primary human foreskin keratinocytes (HFKs) were derived from foreskin samples as previously described [137]. For continuing culture only, primary HFKs were plated on top of the irradiated J2 fibroblast layer. After trypsinizing or thawing, primary HFKs were grown in high glucose DMEM and F12 media supplemented with 10% FBS, 0.4 μg/mL hydrocortisone, 5 μg/mL insulin, 8.4 ng/mL cholera toxin, 24 μg/mL adenine, and 1% L-glutamine. One day after plating, the media was changed to the same as above but with 5% FBS, 10 ng/mL EGF, and 1% penicillin/streptomycin. The media was supplemented with 10 μM Y-27632 dihydrochloride (Chemdea CD0141) to prevent cellular differentiation and senescence [138]. Cells were maintained at 37˚C with 10% CO_2 and passaged every 3–4 days. Y-27632 dihydrochloride was omitted when HFKs were plated for use in experiments.

Nucleic acid transfections

HaCaTs were plated at 60,000 cells per well or HFKs were plated at 90,000 cells per well in a 24-well plate in 500 μL complete media. Cells were transfected with 250 or 500 ng endotoxin-free pGL3 using Lipofectamine 2000 (ThermoFisher 11668) in OptiMEM (Life Technologies). Complexes were made in the following manner: 50 μL OptiMEM was combined with pGL3 (either 250 or 500 ng) or water, and a separate 50 μL of OptiMEM was combined with 2 μL Lipofectamine 2000. Each solution was vortexed, combined, vortexed, and incubated for 15 min at room temperature, prior to dropwise addition of 100 μL of complex to the cells. At various timepoints post-transfection, keratinocytes were washed once with PBS and lysed in 1x RIPA lysis buffer (50 mM Tris-HCl pH 8.0, 150 mM NaCl, 1% NP40, 0.5% sodium deoxycholate, 0.1% SDS), supplemented with 1x reducing SDS-PAGE loading buffer, 1x protease inhibitor cocktail (Sigma P1860), 1mM PMSF and 1x PhosSTOP phosphatase inhibitor cocktail (Roche 04906845001). Samples were then boiled for 5 minutes at 95˚C and stored at -80˚C until gel electrophoresis.

HPV16 production

The R302/5A mutant was generated by site-directed mutagenesis of pXULL-based constructs using the QuikChange XL-II kit and verified by Sanger sequencing [27,139]. Luciferase expressing wt and R302/5A mutant HPV16 pseudovirions were generated as previously described [139]. Briefly, 293TT cells were co-transfected with a pXULL-derived plasmid expressing both L1 and L2. Transfected cells were harvested at 48 hr post-transfection by trypsinization and pelleted/resuspended in PBS + 9.5 mM $MgCl_2$ at 100 μl/10 cm plate, followed by the addition of Brij58 to 0.35%, ammonium sulfate (pH = 9.0) to 25 mM, Benzonase nuclease (Sigma E1014) to 0.3%, and 20U/mL exonuclease V (Epicentre E3105K) with overnight incubation at 37˚C to promote disulfide formation and maturation of capsids. After maturation, 0.17 volumes of 5M NaCl was added and lysates were 1x freeze/thawed to further break apart cellular structures. Lysates were cleared by centrifugation at 3000x g and supernatants were loaded onto discontinuous CsCl gradients made from 4 ml light (1.25 g/ml) CsCl

underlaid with 4 ml heavy (1.4 g/ml) CsCl, dissolved in virus storage buffer (VSB, 25 mM HEPES pH 7.5, 0.5 M NaCl, 1 mM $MgCl_2$). Virions were purified by 18 hr ultracentrifugation at 20,000 rpm at 4˚C in Beckman SW41 Ti rotor/buckets. Viral bands were visible slightly above the gradient interface and were collected by side puncture with a 1.5" 18 gauge needle and 5 ml syringe. CsCl was removed by washing and concentrating 3x in VSB using 100,000 MWCO centrifugation filter units (Sartorius VS04T42). Purified and concentrated virus was stored at -80˚C. Encapsidated pGL3 content (viral genome equivalent, vge) was determined by SYBR green qPCR (Thermo Fisher K0252) against a standard curve dilution series using primers qLuc2-A (ACGATTTTGTGCCAGAGTCC) and qLuc2-B (TATGAGGCAGAGCGACACC), specific for the luciferase gene in the pGL3 plasmid. DNA concentration of the purified virus was determined by measurement of OD260 on a nanodrop spectrophotometer. From this, the capsid content was calculated and the capsid:pGL3 ratios were determined. HPVs do not utilize specific vDNA packaging signals, and the 293TT method used to generate pGL3-containing HPV16 virions results in the promiscuous packaging of chromatinized cellular DNA, in addition to chromatinized pGL3 reporter plasmid [87,140]. The calculated packaging ratio of 11.16 was therefore used to normalize luciferase data in experiments comparing pGL3 delivery via cationic lipid transfection to wildtype HPV infection (Figs 1 and 2).

HPV16 infections

HaCaTs or HFKs were plated at 60,000 or 90,000 cells per well, respectively, in a 24-well plate in 500 μL complete media. Cells were infected the following day with wildtype or R302/5A mutant HPV16 virions at 250 ng or 500 ng vDNA equivalents per well for pIRF3 blotting experiments. Infections were performed at 2e8 vge/well for luciferase experiments. For infection experiments with cationic lipids, HPV16 virions were diluted into 50 μL OptiMEM, and a separate 50 μL of OptiMEM was combined with 3 μL Lipofectamine 2000. Solutions were vortexed, combined, vortexed again and incubated for 15 min at RT prior to addition of the 100 μL onto subconfluent HaCaT or HFK cells plated in 500 μL of the appropriate complete media. Nanopure H_2O was substituted for Lipofectamine 2000 as a control in these experiments. For biochemical inhibition experiments the endosomal acidification and H^+-ATPase inhibitor Bafilomycin A (BafA, Millipore 196000) was used at 100 nM, furin inhibitor decanoyl-RVKR-cmk (dRVKR, Millipore 344930) was used at 25 μM, and γ-secretase inhibitor XXI (XXI, Millipore 565790) was used at 200 nM, as previously described [27]. Neutralizing antibodies H16.V5 specific for HPV16, and B1.A1 specific for BPV1 [141], were provided in cell culture supernatants and used at 1:500 dilutions. Luciferase assays were performed 24 hr post-infection.

Luciferase assay

HPV infected or pGL3 transfected cells were washed once with PBS and lysed in 100 μL reporter lysis buffer (Promega E3971). Luciferase activity was measured on a DTX-800 multimode plate reader (Beckman Coulter) using Luciferase Assay Reagent (Promega E4550). A fraction of each lysate was blotted for GAPDH to normalize luciferase activity.

L2-BirA membrane penetration experiments

HaCaT-GFP-BAP cells were seeded in 24-well plates at 60,000 cells per well. The following day, cells were infected with 250ng L1/well of R302/5A L2-BirA virus [27], complexed +/- Lipofectamine 2000 cationic lipids or media alone, as described above. At indicated times post-infection, samples were processed for reducing SDS-PAGE followed by western blot to detect total and biotinylated GFP.

SDS-PAGE & western blotting

Samples were resolved by SDS-PAGE and transferred onto a 0.45 μm nitrocellulose membrane. Rabbit monoclonal anti-GAPDH (Cell Signaling 2118, 1:5000), mouse monoclonal anti-IRF3 (Abcam 50772, 1:100), rabbit monoclonal anti-STING (Cell Signaling 13647, 1:1000), and rabbit anti-GFP antibody (Clontech 632377, 1:5000) blots were blocked in 5% non-fat powdered milk dissolved in Tris-buffered saline containing 0.1% Tween (TBST). Rabbit monoclonal anti-phospho-IRF3 (Ser396, Cell Signaling 4947, 1:1000) and rabbit monoclonal anti-phospho-STING (Ser366, Cell Signaling 19781, 1:1000), and NeutrAvidin Dylight 800-conjugate (Thermo 22853, 1:10000) blots were blocked in 100% Odyssey blocking buffer (Licor 927–40000). Goat anti-rabbit DyLight 680 (Pierce 35568), goat anti-mouse DyLight 680 (Pierce 35518), goat anti-rabbit DyLight 800 (Pierce 535571) and goat anti-mouse DyLight 800 (Pierce 35521) were used as secondary antibodies at 1:10,000 in either 50% Odyssey blocking buffer/TBST or 5% milk/TBST. Blots were imaged with the Licor Odyssey Infrared Imaging System. Band intensities were quantified by densitometry using ImageJ v1.52a. Briefly, high resolution images were inverted and bands (both pIRF3 and GAPDH for each blot) were carefully boxed to measure the area and mean intensity of each band. An average background intensity value for each blot was used with the appropriate boxed area to subtract background for each specific band. From these values, pIRF3/GAPDH ratios were calculated for each timepoint/condition. Vehicle/VSB control values for each data series were set to "1.00" and relative pIRF3 values were plotted with Prism software.

RNA-seq analysis

RNA was isolated from transfected and infected HFKs using Qiagen's RNeasy Mini Kit (Qiagen 74104). RNA was eluted in 60 μL nuclease-free water, further purified with a TURBO DNA-free Kit (Life Technologies AM1907), then shipped on dry ice to Novogene Corporation (Sacramento, CA). High-quality eukaryotic mRNA libraries were prepared and sequenced on an Illumina platform, yielding >20 million paired-end reads (2x150 bp length) per sample. High-throughput sequencing data were initially processed using the CyVerse Discovery Environment (www.cyverse.org), where FastQC was used for quality screening, HISAT2 [142] for mapping sequences to the human reference genome GRCh38, and featureCounts [143] for generating gene-level read counts (S1 Data). Differential expression analysis of read counts, including library-size correction and statistical testing (accounting for batch effects with the DESeq model, as specified in S2 Data), was performed using the DESeq2 Bioconductor package [144] implemented in R [145] via RStudio's integrated development environment [146]. Lists of differentially expressed genes (S3 Data), with an adjusted P-value < 0.05, were analyzed for functional enrichment (S4 Data) using g:Profiler [147]. Heatmaps and volcano plots where constructed in R using the pheatmap [148] and EnhancedVolcano [149] packages. Microsoft Office Suite and Adobe Illustrator software were used to create and compile additional figures.

Transmission electron microscopy

HPV16 samples were prepared with cationic lipids as described above. Each sample was applied to an ultra-thin carbon film over Lacey Carbon Support Film on 400-mesh copper grids (Ted Pella, Inc.) that were glow discharged for 1 min. Excess solution was blotted with Whatman #1 filter paper and the grid was rapidly stained with 2% uranyl acetate. The uranyl acetate was immediately blotted with Whatman #1 filter paper and rapidly stained with 2% methylamine tungstate. The second stain was immediately blotted away with Whatman #1 filter paper and allowed to air dry. Data were collected on a JEOL 3200FS microscope operated

at 300 kV. Images were acquired at a magnification of 87,000x and 160,000x, and at 1.0 μm underfocus using a Gatan UltraScan 4000 charge-coupled device (CCD) camera.

Statistics

Statistical analyses were performed using Prism 6 (GraphPad Software). Significant differences were determined by one-way ANOVA followed by Dunnett's or Tukey's multiple comparisons test or two-way ANOVA followed by Sidak's multiple comparisons test. An alpha of 0.05 was used to determine the statistical significance of the null-hypothesis.

Supporting information

S1 Fig. Titration of HPV16 infection in HaCaT cells. HaCaT cells were infected with increasing amounts of luciferase-expressing HPV16 pseudovirions (62.5 ng L1/well to 2000 ng L1/well). Luciferase activity was measured 24 hr post-treatment, n = 3 technical replicates, R^2 = 0.987.
(TIFF)

S2 Fig. HPV virion infection does not activate cellular responses to DNA after 24hr. Aggregate gene responses following pGL3 DNA introduced via liposome transfection (red, n = 2 biological replicates) or HPV virion infection (black, n = 3 for Vehicle, 4hr, and 8hr). Preliminary data for 24hr post-infection (blue background, n = 1) indicate cellular responses to DNA remain inactive throughout the initial infection. Metagene $\log_2$ fold change values were computed by aggregating RNA-seq data of all genes within each distinct cellular response cluster (see Fig 3C and 3D). Error bars represent 95% confidence intervals within each gene cluster.
(TIFF)

S1 Data. Gene-level read counts, based on the human reference genome GRCh38, for all RNA-seq samples (n = 13).
(ZIP)

S2 Data. RNA-seq sample metadata including batch effects and experimental design groups.
(RTF)

S3 Data. Differentially expressed genes, with gene symbol and description annotations, as well as the full differential gene expression results in additional sheets.
(XLSX)

S4 Data. Functional enrichment analysis of differentially-expressed genes.
(XLSX)

S5 Data. Clusters of cellular genes up-regulated in response to DNA.
(XLSX)

Acknowledgments

We thank Neil Christensen for the H16.V5 and B1.A1 neutralizing antibodies. We thank Anne Cress for the HaCaT cells and Jana Jandova for isolation and initial culturing of the primary HFKs. We thank Tony Day of the UA ARL Imaging Core-Life Sciences North for assistance with TEM. We thank Matthew Bronnimann for generating and purifying some wildtype HPV16 virion preparations.

Author Contributions

Conceptualization: Brittany L. Uhlorn, Robert Jackson, Koenraad Van Doorslaer, Samuel K. Campos.

Data curation: Robert Jackson, Koenraad Van Doorslaer.

Formal analysis: Brittany L. Uhlorn, Robert Jackson, Shuaizhi Li, Koenraad Van Doorslaer, Samuel K. Campos.

Funding acquisition: Koenraad Van Doorslaer, Samuel K. Campos.

Investigation: Brittany L. Uhlorn, Robert Jackson, Shuaizhi Li, Shauna M. Bratton, Koenraad Van Doorslaer, Samuel K. Campos.

Methodology: Brittany L. Uhlorn, Robert Jackson, Shuaizhi Li, Koenraad Van Doorslaer, Samuel K. Campos.

Project administration: Koenraad Van Doorslaer, Samuel K. Campos.

Software: Robert Jackson, Koenraad Van Doorslaer.

Supervision: Koenraad Van Doorslaer, Samuel K. Campos.

Validation: Brittany L. Uhlorn, Robert Jackson, Shuaizhi Li, Koenraad Van Doorslaer, Samuel K. Campos.

Visualization: Brittany L. Uhlorn, Robert Jackson, Koenraad Van Doorslaer, Samuel K. Campos.

Writing – original draft: Brittany L. Uhlorn, Robert Jackson, Koenraad Van Doorslaer, Samuel K. Campos.

Writing – review & editing: Brittany L. Uhlorn, Robert Jackson, Koenraad Van Doorslaer, Samuel K. Campos.

References

1. Schiffman M, Castle PE, Jeronimo J, Rodriguez AC, Wacholder S. 2007. Human papillomavirus and cervical cancer. Lancet 370:890–907. https://doi.org/10.1016/S0140-6736(07)61416-0 PMID: 17826171
2. Graham SV. 2017. Keratinocyte Differentiation-Dependent Human Papillomavirus Gene Regulation. Viruses 9. https://doi.org/10.3390/v9090245 PMID: 28867768
3. Moody C. 2017. Mechanisms by which HPV Induces a Replication Competent Environment in Differentiating Keratinocytes. Viruses 9. https://doi.org/10.3390/v9090261 PMID: 28925973
4. Kajitani N, Satsuka A, Kawate A, Sakai H. 2012. Productive Lifecycle of Human Papillomaviruses that Depends Upon Squamous Epithelial Differentiation. Front Microbiol 3:152. https://doi.org/10.3389/fmicb.2012.00152 PMID: 22536200
5. Doorbar J, Quint W, Banks L, Bravo IG, Stoler M, Broker TR, et al. 2012. The biology and life-cycle of human papillomaviruses. Vaccine 30 Suppl 5:F55–70. https://doi.org/10.1016/j.vaccine.2012.06.083 PMID: 23199966
6. Schiffman M, Doorbar J, Wentzensen N, de Sanjose S, Fakhry C, Monk BJ, et al. 2016. Carcinogenic human papillomavirus infection. Nat Rev Dis Primers 2:16086. https://doi.org/10.1038/nrdp.2016.86 PMID: 27905473
7. Schiffman M, Herrero R, Desalle R, Hildesheim A, Wacholder S, Rodriguez AC, et al. 2005. The carcinogenicity of human papillomavirus types reflects viral evolution. Virology 337:76–84. https://doi.org/10.1016/j.virol.2005.04.002 PMID: 15914222
8. Campos SK. 2017. Subcellular Trafficking of the Papillomavirus Genome during Initial Infection: The Remarkable Abilities of Minor Capsid Protein L2. Viruses 9. https://doi.org/10.3390/v9120370 PMID: 29207511

9. DiGiuseppe S, Bienkowska-Haba M, Guion LG, Sapp M. 2017. Cruising the cellular highways: How human papillomavirus travels from the surface to the nucleus. Virus Res 231:1–9. https://doi.org/10.1016/j.virusres.2016.10.015 PMID: 27984059

10. Mikulicic S, Florin L. 2019. The endocytic trafficking pathway of oncogenic papillomaviruses. Papillomavirus Res 7:135–137. https://doi.org/10.1016/j.pvr.2019.03.004 PMID: 30946955

11. Bronnimann MP, Calton CM, Chiquette SF, Li S, Lu M, Chapman JA, et al. 2016. Furin Cleavage of L2 During Papillomavirus Infection: Minimal Dependence on Cyclophilins. J Virol https://doi.org/10.1128/JVI.00038-16 PMID: 27122588

12. Cerqueira C, Samperio Ventayol P, Vogeley C, Schelhaas M. 2015. Kallikrein-8 Proteolytically Processes Human Papillomaviruses in the Extracellular Space To Facilitate Entry into Host Cells. J Virol 89:7038–7052. https://doi.org/10.1128/JVI.00234-15 PMID: 25926655

13. Richards RM, Lowy DR, Schiller JT, Day PM. 2006. Cleavage of the papillomavirus minor capsid protein, L2, at a furin consensus site is necessary for infection. Proc Natl Acad Sci U S A 103:1522–1527. https://doi.org/10.1073/pnas.0508815103 PMID: 16432208

14. Becker M, Greune L, Schmidt MA, Schelhaas M. 2018. Extracellular conformational changes in the capsid of human papillomaviruses contribute to asynchronous uptake into host cells. J Virol https://doi.org/10.1128/JVI.02106-17 PMID: 29593032

15. Cerqueira C, Liu Y, Kuhling L, Chai W, Hafezi W, van Kuppevelt TH, et al. 2013. Heparin increases the infectivity of Human Papillomavirus type 16 independent of cell surface proteoglycans and induces L1 epitope exposure. Cell Microbiol 15:1818–1836. https://doi.org/10.1111/cmi.12150 PMID: 23601855

16. Richards KF, Bienkowska-Haba M, Dasgupta J, Chen XS, Sapp M. 2013. Multiple heparan sulfate binding site engagements are required for the infectious entry of human papillomavirus type 16. J Virol 87:11426–11437. https://doi.org/10.1128/JVI.01721-13 PMID: 23966387

17. Mikulicic S, Finke J, Boukhallouk F, Wustenhagen E, Sons D, Homsi Y, et al. 2019. ADAM17-dependent signaling is required for oncogenic human papillomavirus entry platform assembly. Elife 8. https://doi.org/10.7554/eLife.44345 PMID: 31107240

18. Bannach C, Brinkert P, Kuhling L, Greune L, Schmidt MA, Schelhaas M. 2020. Epidermal growth factor receptor and Abl2 kinase regulate distinct steps of Human papillomavirus type 16 endocytosis. J Virol https://doi.org/10.1128/JVI.02143-19 PMID: 32188731

19. Surviladze Z, Dziduszko A, Ozbun MA. 2012. Essential roles for soluble virion-associated heparan sulfonated proteoglycans and growth factors in human papillomavirus infections. PLoS Pathog 8: e1002519. https://doi.org/10.1371/journal.ppat.1002519 PMID: 22346752

20. Surviladze Z, Sterk RT, DeHaro SA, Ozbun MA. 2013. Cellular entry of human papillomavirus type 16 involves activation of the phosphatidylinositol 3-kinase/Akt/mTOR pathway and inhibition of autophagy. J Virol 87:2508–2517. https://doi.org/10.1128/JVI.02319-12 PMID: 23255786

21. Gräßel L, Fast LA, Scheffer KD, Boukhallouk F, Spoden GA, Tenzer S, et al. 2016. The CD63-Syntenin-1 Complex Controls Post-Endocytic Trafficking of Oncogenic Human Papillomaviruses. Sci Rep 6:32337. https://doi.org/10.1038/srep32337 PMID: 27578500

22. Schelhaas M, Shah B, Holzer M, Blattmann P, Kuhling L, Day PM, et al. 2012. Entry of human papillomavirus type 16 by actin-dependent, clathrin- and lipid raft-independent endocytosis. PLoS Pathog 8: e1002657. https://doi.org/10.1371/journal.ppat.1002657 PMID: 22536154

23. Day PM, Thompson CD, Schowalter RM, Lowy DR, Schiller JT. 2013. Identification of a role for the trans-Golgi network in human papillomavirus 16 pseudovirus infection. J Virol 87:3862–3870. https://doi.org/10.1128/JVI.03222-12 PMID: 23345514

24. Lipovsky A, Popa A, Pimienta G, Wyler M, Bhan A, Kuruvilla L, et al. 2013. Genome-wide siRNA screen identifies the retromer as a cellular entry factor for human papillomavirus. Proc Natl Acad Sci U S A 110:7452–7457. https://doi.org/10.1073/pnas.1302164110 PMID: 23569269

25. Popa A, Zhang W, Harrison MS, Goodner K, Kazakov T, Goodwin EC, et al. 2015. Direct binding of retromer to human papillomavirus type 16 minor capsid protein L2 mediates endosome exit during viral infection. PLoS Pathog 11:e1004699. https://doi.org/10.1371/journal.ppat.1004699 PMID: 25693203

26. Zhang W, Kazakov T, Popa A, DiMaio D. 2014. Vesicular trafficking of incoming human papillomavirus 16 to the Golgi apparatus and endoplasmic reticulum requires gamma-secretase activity. MBio 5: e01777–01714. https://doi.org/10.1128/mBio.01777-14 PMID: 25227470

27. Calton CM, Bronnimann MP, Manson AR, Li S, Chapman JA, Suarez-Berumen M, et al. 2017. Translocation of the papillomavirus L2/vDNA complex across the limiting membrane requires the onset of mitosis. PLoS Pathog 13:e1006200. https://doi.org/10.1371/journal.ppat.1006200 PMID: 28463988

28. Bronnimann MP, Chapman JA, Park CK, Campos SK. 2013. A transmembrane domain and GxxxG motifs within L2 are essential for papillomavirus infection. J Virol 87:464–473. https://doi.org/10.1128/JVI.01539-12 PMID: 23097431

29. DiGiuseppe S, Keiffer TR, Bienkowska-Haba M, Luszczek W, Guion LG, Muller M, et al. 2015. Topography of the Human Papillomavirus Minor Capsid Protein L2 during Vesicular Trafficking of Infectious Entry. J Virol 89:10442–10452. https://doi.org/10.1128/JVI.01588-15 PMID: 26246568

30. Inoue T, Zhang P, Zhang W, Goodner-Bingham K, Dupzyk A, DiMaio D, et al. 2018. gamma-Secretase promotes membrane insertion of the human papillomavirus L2 capsid protein during virus infection. J Cell Biol 217:3545–3559. https://doi.org/10.1083/jcb.201804171 PMID: 30006461

31. Zhang P, Monteiro da Silva G, Deatherage C, Burd C, DiMaio D. 2018. Cell-Penetrating Peptide Mediates Intracellular Membrane Passage of Human Papillomavirus L2 Protein to Trigger Retrograde Trafficking. Cell 174:1465–1476 e1413. https://doi.org/10.1016/j.cell.2018.07.031 PMID: 30122350

32. Bergant M, Peternel S, Pim D, Broniarczyk J, Banks L. 2017. Characterizing the spatio-temporal role of sorting nexin 17 in human papillomavirus trafficking. J Gen Virol 98:715–725. https://doi.org/10.1099/jgv.0.000734 PMID: 28475030

33. Aydin I, Villalonga-Planells R, Greune L, Bronnimann MP, Calton CM, Becker M, et al. 2017. A central region in the minor capsid protein of papillomaviruses facilitates viral genome tethering and membrane penetration for mitotic nuclear entry. PLoS Pathog 13:e1006308. https://doi.org/10.1371/journal.ppat.1006308 PMID: 28464022

34. Day PM, Weisberg AS, Thompson CD, Hughes MM, Pang YY, Lowy DR, et al. 2019. Human Papillomavirus 16 Capsids Mediate Nuclear Entry during Infection. J Virol 93. https://doi.org/10.1128/JVI.00454-19 PMID: 31092566

35. DiGiuseppe S, Luszczek W, Keiffer TR, Bienkowska-Haba M, Guion LG, Sapp MJ. 2016. Incoming human papillomavirus type 16 genome resides in a vesicular compartment throughout mitosis. Proc Natl Acad Sci U S A 113:6289–6294. https://doi.org/10.1073/pnas.1600638113 PMID: 27190090

36. DiGiuseppe S, Bienkowska-Haba M, Guion LGM, Keiffer TR, Sapp M. 2017. Human Papillomavirus Major Capsid Protein L1 Remains Associated with the Incoming Viral Genome throughout the Entry Process. J Virol 91. https://doi.org/10.1128/JVI.00537-17 PMID: 28566382

37. Guion L, Bienkowska-Haba M, DiGiuseppe S, Florin L, Sapp M. 2019. PML nuclear body-residing proteins sequentially associate with HPV genome after infectious nuclear delivery. PLoS Pathog 15:e1007590. https://doi.org/10.1371/journal.ppat.1007590 PMID: 30802273

38. Day PM, Baker CC, Lowy DR, Schiller JT. 2004. Establishment of papillomavirus infection is enhanced by promyelocytic leukemia protein (PML) expression. Proc Natl Acad Sci U S A 101:14252–14257. https://doi.org/10.1073/pnas.0404229101 PMID: 15383670

39. Kumar CS, Dey D, Ghosh S, Banerjee M. 2018. Breach: Host Membrane Penetration and Entry by Nonenveloped Viruses. Trends Microbiol 26:525–537. https://doi.org/10.1016/j.tim.2017.09.010 PMID: 29079499

40. Moyer CL, Nemerow GR. 2011. Viral weapons of membrane destruction: variable modes of membrane penetration by non-enveloped viruses. Curr Opin Virol 1:44–49. https://doi.org/10.1016/j.coviro.2011.05.002 PMID: 21804909

41. Tsai B. 2007. Penetration of nonenveloped viruses into the cytoplasm. Annu Rev Cell Dev Biol 23:23–43. https://doi.org/10.1146/annurev.cellbio.23.090506.123454 PMID: 17456018

42. DiGiuseppe S, Bienkowska-Haba M, Sapp M. 2016. Human Papillomavirus Entry: Hiding in a Bubble. J Virol 90:8032–8035. https://doi.org/10.1128/JVI.01065-16 PMID: 27412595

43. Spriggs CC, Harwood MC, Tsai B. 2019. How non-enveloped viruses hijack host machineries to cause infection. Adv Virus Res 104:97–122. https://doi.org/10.1016/bs.aivir.2019.05.002 PMID: 31439154

44. Takeuchi O, Akira S. 2010. Pattern recognition receptors and inflammation. Cell 140:805–820. https://doi.org/10.1016/j.cell.2010.01.022 PMID: 20303872

45. Gong T, Liu L, Jiang W, Zhou R. 2020. DAMP-sensing receptors in sterile inflammation and inflammatory diseases. Nat Rev Immunol 20:95–112. https://doi.org/10.1038/s41577-019-0215-7 PMID: 31558839

46. Patel S. 2018. Danger-Associated Molecular Patterns (DAMPs): the Derivatives and Triggers of Inflammation. Curr Allergy Asthma Rep 18:63. https://doi.org/10.1007/s11882-018-0817-3 PMID: 30267163

47. Wu J, Chen ZJ. 2014. Innate immune sensing and signaling of cytosolic nucleic acids. Annu Rev Immunol 32:461–488. https://doi.org/10.1146/annurev-immunol-032713-120156 PMID: 24655297

48. Li T, Chen ZJ. 2018. The cGAS-cGAMP-STING pathway connects DNA damage to inflammation, senescence, and cancer. J Exp Med 215:1287–1299. https://doi.org/10.1084/jem.20180139 PMID: 29622565

49. Chen Q, Sun L, Chen ZJ. 2016. Regulation and function of the cGAS-STING pathway of cytosolic DNA sensing. Nat Immunol 17:1142–1149. https://doi.org/10.1038/ni.3558 PMID: 27648547

50. Tao J, Zhou X, Jiang Z. 2016. cGAS-cGAMP-STING: The three musketeers of cytosolic DNA sensing and signaling. IUBMB Life 68:858–870. https://doi.org/10.1002/iub.1566 PMID: 27706894

51. Ablasser A, Chen ZJ. 2019. cGAS in action: Expanding roles in immunity and inflammation. Science 363. https://doi.org/10.1126/science.aat8657 PMID: 30846571

52. Motwani M, Pesiridis S, Fitzgerald KA. 2019. DNA sensing by the cGAS-STING pathway in health and disease. Nat Rev Genet 20:657–674. https://doi.org/10.1038/s41576-019-0151-1 PMID: 31358977

53. Ablasser A, Schmid-Burgk JL, Hemmerling I, Horvath GL, Schmidt T, Latz E, et al. 2013. Cell intrinsic immunity spreads to bystander cells via the intercellular transfer of cGAMP. Nature 503:530–534. https://doi.org/10.1038/nature12640 PMID: 24077100

54. Sun L, Wu J, Du F, Chen X, Chen ZJ. 2013. Cyclic GMP-AMP synthase is a cytosolic DNA sensor that activates the type I interferon pathway. Science 339:786–791. https://doi.org/10.1126/science.1232458 PMID: 23258413

55. Ishikawa H, Barber GN. 2008. STING is an endoplasmic reticulum adaptor that facilitates innate immune signalling. Nature 455:674–678. https://doi.org/10.1038/nature07317 PMID: 18724357

56. Yin Q, Tian Y, Kabaleeswaran V, Jiang X, Tu D, Eck MJ, et al. 2012. Cyclic di-GMP sensing via the innate immune signaling protein STING. Mol Cell 46:735–745. https://doi.org/10.1016/j.molcel.2012.05.029 PMID: 22705373

57. Ishikawa H, Ma Z, Barber GN. 2009. STING regulates intracellular DNA-mediated, type I interferon-dependent innate immunity. Nature 461:788–792. https://doi.org/10.1038/nature08476 PMID: 19776740

58. Saitoh T, Fujita N, Hayashi T, Takahara K, Satoh T, Lee H, et al. 2009. Atg9a controls dsDNA-driven dynamic translocation of STING and the innate immune response. Proc Natl Acad Sci U S A 106:20842–20846. https://doi.org/10.1073/pnas.0911267106 PMID: 19926846

59. Shang G, Zhang C, Chen ZJ, Bai XC, Zhang X. 2019. Cryo-EM structures of STING reveal its mechanism of activation by cyclic GMP-AMP. Nature 567:389–393. https://doi.org/10.1038/s41586-019-0998-5 PMID: 30842659

60. Zhang C, Shang G, Gui X, Zhang X, Bai XC, Chen ZJ. 2019. Structural basis of STING binding with and phosphorylation by TBK1. Nature 567:394–398. https://doi.org/10.1038/s41586-019-1000-2 PMID: 30842653

61. Tanaka Y, Chen ZJ. 2012. STING specifies IRF3 phosphorylation by TBK1 in the cytosolic DNA signaling pathway. Sci Signal 5:ra20. https://doi.org/10.1126/scisignal.2002521 PMID: 22394562

62. Reinert LS, Lopusna K, Winther H, Sun C, Thomsen MK, Nandakumar R, et al. 2016. Sensing of HSV-1 by the cGAS-STING pathway in microglia orchestrates antiviral defence in the CNS. Nat Commun 7:13348. https://doi.org/10.1038/ncomms13348 PMID: 27830700

63. Lam E, Stein S, Falck-Pedersen E. 2014. Adenovirus detection by the cGAS/STING/TBK1 DNA sensing cascade. J Virol 88:974–981. https://doi.org/10.1128/JVI.02702-13 PMID: 24198409

64. Xia P, Ye B, Wang S, Zhu X, Du Y, Xiong Z, et al. 2016. Glutamylation of the DNA sensor cGAS regulates its binding and synthase activity in antiviral immunity. Nat Immunol 17:369–378. https://doi.org/10.1038/ni.3356 PMID: 26829768

65. Dai P, Wang W, Cao H, Avogadri F, Dai L, Drexler I, et al. 2014. Modified vaccinia virus Ankara triggers type I IFN production in murine conventional dendritic cells via a cGAS/STING-mediated cytosolic DNA-sensing pathway. PLoS Pathog 10:e1003989. https://doi.org/10.1371/journal.ppat.1003989 PMID: 24743339

66. Ma Z, Jacobs SR, West JA, Stopford C, Zhang Z, Davis Z, et al. 2015. Modulation of the cGAS-STING DNA sensing pathway by gammaherpesviruses. Proc Natl Acad Sci U S A 112:E4306–4315. https://doi.org/10.1073/pnas.1503831112 PMID: 26199418

67. Fu YZ, Su S, Gao YQ, Wang PP, Huang ZF, Hu MM, et al. 2017. Human Cytomegalovirus Tegument Protein UL82 Inhibits STING-Mediated Signaling to Evade Antiviral Immunity. Cell Host Microbe 21:231–243. https://doi.org/10.1016/j.chom.2017.01.001 PMID: 28132838

68. Paijo J, Doring M, Spanier J, Grabski E, Nooruzzaman M, Schmidt T, et al. 2016. cGAS Senses Human Cytomegalovirus and Induces Type I Interferon Responses in Human Monocyte-Derived Cells. PLoS Pathog 12:e1005546. https://doi.org/10.1371/journal.ppat.1005546 PMID: 27058035

69. Garcia-Belmonte R, Perez-Nunez D, Pittau M, Richt JA, Revilla Y. 2019. African Swine Fever Virus Armenia/07 Virulent Strain Controls Interferon Beta Production through the cGAS-STING Pathway. J Virol 93. https://doi.org/10.1128/JVI.02298-18 PMID: 30918080

70. Lau L, Gray EE, Brunette RL, Stetson DB. 2015. DNA tumor virus oncogenes antagonize the cGAS-STING DNA-sensing pathway. Science 350:568–571. https://doi.org/10.1126/science.aab3291 PMID: 26405230

71. Ronco LV, Karpova AY, Vidal M, Howley PM. 1998. Human papillomavirus 16 E6 oncoprotein binds to interferon regulatory factor-3 and inhibits its transcriptional activity. Genes Dev 12:2061–2072. https://doi.org/10.1101/gad.12.13.2061 PMID: 9649509

72. Shaikh MH, Bortnik V, McMillan NA, Idris A. 2019. cGAS-STING responses are dampened in high-risk HPV type 16 positive head and neck squamous cell carcinoma cells. Microb Pathog 132:162–165. https://doi.org/10.1016/j.micpath.2019.05.004 PMID: 31054871

73. Chang YE, Pena L, Sen GC, Park JK, Laimins LA. 2002. Long-term effect of interferon on keratinocytes that maintain human papillomavirus type 31. J Virol 76:8864–8874. https://doi.org/10.1128/jvi.76.17.8864-8874.2002 PMID: 12163606

74. Herdman MT, Pett MR, Roberts I, Alazawi WO, Teschendorff AE, Zhang XY, et al. 2006. Interferon-beta treatment of cervical keratinocytes naturally infected with human papillomavirus 16 episomes promotes rapid reduction in episome numbers and emergence of latent integrants. Carcinogenesis 27:2341–2353. https://doi.org/10.1093/carcin/bgl172 PMID: 16973673

75. Lace MJ, Anson JR, Haugen TH, Dierdorff JM, Turek LP. 2015. Interferon treatment of human keratinocytes harboring extrachromosomal, persistent HPV-16 plasmid genomes induces de novo viral integration. Carcinogenesis 36:151–159. https://doi.org/10.1093/carcin/bgu236 PMID: 25416558

76. Liu H, Golji J, Brodeur LK, Chung FS, Chen JT, deBeaumont RS, et al. 2019. Tumor-derived IFN triggers chronic pathway agonism and sensitivity to ADAR loss. Nat Med 25:95–102. https://doi.org/10.1038/s41591-018-0302-5 PMID: 30559422

77. Terenzi F, Saikia P, Sen GC. 2008. Interferon-inducible protein, P56, inhibits HPV DNA replication by binding to the viral protein E1. EMBO J 27:3311–3321. https://doi.org/10.1038/emboj.2008.241 PMID: 19008854

78. Ferreira AR, Ramalho AC, Marques M, Ribeiro D. 2020. The Interplay between Antiviral Signalling and Carcinogenesis in Human Papillomavirus Infections. Cancers (Basel) 12. https://doi.org/10.3390/cancers12030646 PMID: 32164347

79. James CD, Fontan CT, Otoa R, Das D, Prabhakar AT, Wang X, et al. 2020. Human Papillomavirus 16 E6 and E7 Synergistically Repress Innate Immune Gene Transcription. mSphere 5. https://doi.org/10.1128/mSphere.00828-19 PMID: 31915229

80. Lo Cigno I, Calati F, Borgogna C, Zevini A, Albertini S, Martuscelli L, et al. 2020. Human Papillomavirus E7 Oncoprotein Subverts Host Innate Immunity via SUV39H1-Mediated Epigenetic Silencing of Immune Sensor Genes. J Virol 94. https://doi.org/10.1128/JVI.01812-19 PMID: 31776268

81. Scott ML, Woodby BL, Ulicny J, Raikhy G, Orr AW, Songock WK, et al. 2020. Human Papillomavirus 16 E5 Inhibits Interferon Signaling and Supports Episomal Viral Maintenance. J Virol 94. https://doi.org/10.1128/JVI.01582-19 PMID: 31666385

82. Boukamp P, Petrussevska RT, Breitkreutz D, Hornung J, Markham A, Fusenig NE. 1988. Normal keratinization in a spontaneously immortalized aneuploid human keratinocyte cell line. J Cell Biol 106:761–771. https://doi.org/10.1083/jcb.106.3.761 PMID: 2450098

83. Kim JA, Park SK, Seo SW, Lee CH, Shin OS. 2017. STING Is Involved in Antiviral Immune Response against VZV Infection via the Induction of Type I and III IFN Pathways. J Invest Dermatol 137:2101–2109. https://doi.org/10.1016/j.jid.2017.03.041 PMID: 28647346

84. Skouboe MK, Knudsen A, Reinert LS, Boularan C, Lioux T, Perouzel E, et al. 2018. STING agonists enable antiviral cross-talk between human cells and confer protection against genital herpes in mice. PLoS Pathog 14:e1006976. https://doi.org/10.1371/journal.ppat.1006976 PMID: 29608601

85. Uhlorn BL, Gamez ER, Li S, Campos SK. 2020. Attenuation of cGAS/STING Activity During Mitosis. Life Sci Alliance 3:e201900636. https://doi.org/10.26508/lsa.201900636 PMID: 32661021

86. Cerqueira C, Schiller JT. 2017. Papillomavirus assembly: An overview and perspectives. Virus Res 231:103–107. https://doi.org/10.1016/j.virusres.2016.11.010 PMID: 27840111

87. Buck CB, Pastrana DV, Lowy DR, Schiller JT. 2005. Generation of HPV pseudovirions using transfection and their use in neutralization assays. Methods Mol Med 119:445–462. https://doi.org/10.1385/1-59259-982-6:445 PMID: 16350417

88. Gao D, Wu J, Wu YT, Du F, Aroh C, Yan N, et al. 2013. Cyclic GMP-AMP synthase is an innate immune sensor of HIV and other retroviruses. Science 341:903–906. https://doi.org/10.1126/science.1240933 PMID: 23929945

89. Lahaye X, Satoh T, Gentili M, Cerboni S, Conrad C, Hurbain I, et al. 2013. The capsids of HIV-1 and HIV-2 determine immune detection of the viral cDNA by the innate sensor cGAS in dendritic cells. Immunity 39:1132–1142. https://doi.org/10.1016/j.immuni.2013.11.002 PMID: 24269171

90. Chesnoy S, Huang L. 2000. Structure and function of lipid-DNA complexes for gene delivery. Annu Rev Biophys Biomol Struct 29:27–47. https://doi.org/10.1146/annurev.biophys.29.1.27 PMID: 10940242

91. Stebelska K, Dubielecka PM, Sikorski AF. 2005. The effect of PS content on the ability of natural membranes to fuse with positively charged liposomes and lipoplexes. J Membr Biol 206:203–214. https://doi.org/10.1007/s00232-005-0793-0 PMID: 16456715

92. Wattiaux R, Jadot M, Warnier-Pirotte MT, Wattiaux-De Coninck S. 1997. Cationic lipids destabilize lysosomal membrane in vitro. FEBS Lett 417:199–202. https://doi.org/10.1016/s0014-5793(97)01283-0 PMID: 9395295

93. DiGiuseppe S, Bienkowska-Haba M, Hilbig L, Sapp M. 2014. The nuclear retention signal of HPV16 L2 protein is essential for incoming viral genome to transverse the trans-Golgi network. Virology 458–459:93–105. https://doi.org/10.1016/j.virol.2014.04.024 PMID: 24928042

94. Li S, Bronnimann MP, Williams SJ, Campos SK. 2019. Glutathione contributes to efficient post-Golgi trafficking of incoming HPV16 genome. PLoS One 14:e0225496. https://doi.org/10.1371/journal.pone.0225496 PMID: 31743367

95. Medzhitov R. 2007. Recognition of microorganisms and activation of the immune response. Nature 449:819–826. https://doi.org/10.1038/nature06246 PMID: 17943118

96. Ma Z, Ni G, Damania B. 2018. Innate Sensing of DNA Virus Genomes. Annu Rev Virol 5:341–362. https://doi.org/10.1146/annurev-virology-092917-043244 PMID: 30265633

97. Tummers B, Goedemans R, Pelascini LP, Jordanova ES, van Esch EM, Meyers C, et al. 2015. The interferon-related developmental regulator 1 is used by human papillomavirus to suppress NFkappaB activation. Nat Commun 6:6537. https://doi.org/10.1038/ncomms7537 PMID: 26055519

98. Albertini S, Lo Cigno I, Calati F, De Andrea M, Borgogna C, Dell'Oste V, et al. 2018. HPV18 Persistence Impairs Basal and DNA Ligand-Mediated IFN-beta and IFN-lambda1 Production through Transcriptional Repression of Multiple Downstream Effectors of Pattern Recognition Receptor Signaling. J Immunol 200:2076–2089. https://doi.org/10.4049/jimmunol.1701536 PMID: 29386255

99. Stanley MA. 2012. Epithelial cell responses to infection with human papillomavirus. Clin Microbiol Rev 25:215–222. https://doi.org/10.1128/CMR.05028-11 PMID: 22491770

100. Bienkowska-Haba M, Luszczek W, Keiffer TR, Guion LGM, DiGiuseppe S, Scott RS, et al. 2017. Incoming human papillomavirus 16 genome is lost in PML protein-deficient HaCaT keratinocytes. Cell Microbiol 19. https://doi.org/10.1111/cmi.12708 PMID: 27860076

101. Luff JA, Yuan H, Kennedy D, Schlegel R, Felsburg P, Moore PF. 2014. Keratinocyte antiviral response to Poly(dA:dT) stimulation and papillomavirus infection in a canine model of X-linked severe combined immunodeficiency. PLoS One 9:e102033. https://doi.org/10.1371/journal.pone.0102033 PMID: 25025687

102. Grandvaux N, Servant MJ, tenOever B, Sen GC, Balachandran S, Barber GN, et al. 2002. Transcriptional profiling of interferon regulatory factor 3 target genes: direct involvement in the regulation of interferon-stimulated genes. J Virol 76:5532–5539. https://doi.org/10.1128/jvi.76.11.5532-5539.2002 PMID: 11991981

103. Helbig KJ, Ruszkiewicz A, Lanford RE, Berzsenyi MD, Harley HA, McColl SR, et al. 2009. Differential expression of the CXCR3 ligands in chronic hepatitis C virus (HCV) infection and their modulation by HCV in vitro. J Virol 83:836–846. https://doi.org/10.1128/JVI.01388-08 PMID: 18987152

104. Brownell J, Bruckner J, Wagoner J, Thomas E, Loo YM, Gale M Jr., et al. 2014. Direct, interferon-independent activation of the CXCL10 promoter by NF-kappaB and interferon regulatory factor 3 during hepatitis C virus infection. J Virol 88:1582–1590. https://doi.org/10.1128/JVI.02007-13 PMID: 24257594

105. Durfee LA, Lyon N, Seo K, Huibregtse JM. 2010. The ISG15 conjugation system broadly targets newly synthesized proteins: implications for the antiviral function of ISG15. Mol Cell 38:722–732. https://doi.org/10.1016/j.molcel.2010.05.002 PMID: 20542004

106. Dufour JH, Dziejman M, Liu MT, Leung JH, Lane TE, Luster AD. 2002. IFN-gamma-inducible protein 10 (IP-10; CXCL10)-deficient mice reveal a role for IP-10 in effector T cell generation and trafficking. J Immunol 168:3195–3204. https://doi.org/10.4049/jimmunol.168.7.3195 PMID: 11907072

107. Clark-Lewis I, Mattioli I, Gong JH, Loetscher P. 2003. Structure-function relationship between the human chemokine receptor CXCR3 and its ligands. J Biol Chem 278:289–295. https://doi.org/10.1074/jbc.M209470200 PMID: 12417585

108. Wang W, Uberoi A, Spurgeon M, Gronski E, Majerciak V, Lobanov A, et al. 2020. Stress keratin 17 enhances papillomavirus infection-induced disease by downregulating T cell recruitment. PLoS Pathog 16:e1008206. https://doi.org/10.1371/journal.ppat.1008206 PMID: 31968015

109. Lo Cigno I, De Andrea M, Borgogna C, Albertini S, Landini MM, Peretti A, et al. 2015. The Nuclear DNA Sensor IFI16 Acts as a Restriction Factor for Human Papillomavirus Replication through Epigenetic Modifications of the Viral Promoters. J Virol 89:7506–7520. https://doi.org/10.1128/JVI.00013-15 PMID: 25972554

110. Riva G, Biolatti M, Pecorari G, Dell'Oste V, Landolfo S. 2019. PYHIN Proteins and HPV: Role in the Pathogenesis of Head and Neck Squamous Cell Carcinoma. Microorganisms 8. https://doi.org/10.3390/microorganisms8010014 PMID: 31861809

111. Park JS, Kim EJ, Kwon HJ, Hwang ES, Namkoong SE, Um SJ. 2000. Inactivation of interferon regulatory factor-1 tumor suppressor protein by HPV E7 oncoprotein. Implication for the E7-mediated immune evasion mechanism in cervical carcinogenesis. J Biol Chem 275:6764–6769. https://doi.org/10.1074/jbc.275.10.6764 PMID: 10702232

112. Perea SE, Massimi P, Banks L. 2000. Human papillomavirus type 16 E7 impairs the activation of the interferon regulatory factor-1. Int J Mol Med 5:661–666. https://doi.org/10.3892/ijmm.5.6.661 PMID: 10812019

113. Lee HS, Lee JH, Park YM. 2017. E7 protein of cutaneous human papillomavirus attenuates viperin expression in human keratinocytes. J Dermatol Sci 87:91–94. https://doi.org/10.1016/j.jdermsci.2017.02.001 PMID: 28242342

114. Wang H, Mo P, Ren S, Yan C. 2010. Activating transcription factor 3 activates p53 by preventing E6-associated protein from binding to E6. J Biol Chem 285:13201–13210. https://doi.org/10.1074/jbc.M109.058669 PMID: 20167600

115. Guan KL, Jenkins CW, Li Y, Nichols MA, Wu X, O'Keefe CL, et al. 1994. Growth suppression by p18, a p16INK4/MTS1- and p14INK4B/MTS2-related CDK6 inhibitor, correlates with wild-type pRb function. Genes Dev 8:2939–2952. https://doi.org/10.1101/gad.8.24.2939 PMID: 8001816

116. Wang X, Meyers C, Guo M, Zheng ZM. 2011. Upregulation of p18Ink4c expression by oncogenic HPV E6 via p53-miR-34a pathway. Int J Cancer 129:1362–1372. https://doi.org/10.1002/ijc.25800 PMID: 21128241

117. Wang S, El-Deiry WS. 2003. TRAIL and apoptosis induction by TNF-family death receptors. Oncogene 22:8628–8633. https://doi.org/10.1038/sj.onc.1207232 PMID: 14634624

118. Kabsch K, Alonso A. 2002. The human papillomavirus type 16 E5 protein impairs TRAIL- and FasL-mediated apoptosis in HaCaT cells by different mechanisms. J Virol 76:12162–12172. https://doi.org/10.1128/jvi.76.23.12162-12172.2002 PMID: 12414956

119. Kabsch K, Mossadegh N, Kohl A, Komposch G, Schenkel J, Alonso A, et al. 2004. The HPV-16 E5 protein inhibits TRAIL- and FasL-mediated apoptosis in human keratinocyte raft cultures. Intervirology 47:48–56. https://doi.org/10.1159/000076642 PMID: 15044836

120. Mackenzie KJ, Carroll P, Martin CA, Murina O, Fluteau A, Simpson DJ, et al. 2017. cGAS surveillance of micronuclei links genome instability to innate immunity. Nature 548:461–465. https://doi.org/10.1038/nature23449 PMID: 28738408

121. Zierhut C, Yamaguchi N, Paredes M, Luo JD, Carroll T, Funabiki H. 2019. The Cytoplasmic DNA Sensor cGAS Promotes Mitotic Cell Death. Cell 178:302–315 e323. https://doi.org/10.1016/j.cell.2019.05.035 PMID: 31299200

122. Burleigh K, Maltbaek JH, Cambier S, Green R, Gale M Jr., James RC, et al. 2020. Human DNA-PK activates a STING-independent DNA sensing pathway. Sci Immunol 5. https://doi.org/10.1126/sciimmunol.aba4219 PMID: 31980485

123. Pennington MR, Saha A, Painter DF, Gavazzi C, Ismail AM, Zhou X, et al. 2019. Disparate Entry of Adenoviruses Dictates Differential Innate Immune Responses on the Ocular Surface. Microorganisms 7. https://doi.org/10.3390/microorganisms7090351 PMID: 31540200

124. Teigler JE, Kagan JC, Barouch DH. 2014. Late endosomal trafficking of alternative serotype adenovirus vaccine vectors augments antiviral innate immunity. J Virol 88:10354–10363. https://doi.org/10.1128/JVI.00936-14 PMID: 24991003

125. Lee JS, Ismail AM, Lee JY, Zhou X, Materne EC, Chodosh J, et al. 2019. Impact of dynamin 2 on adenovirus nuclear entry. Virology 529:43–56. https://doi.org/10.1016/j.virol.2019.01.008 PMID: 30660774

126. Stuart JD, Holm GH, Boehme KW. 2018. Differential Delivery of Genomic Double-Stranded RNA Causes Reovirus Strain-Specific Differences in Interferon Regulatory Factor 3 Activation. J Virol 92. https://doi.org/10.1128/JVI.01947-17 PMID: 29437975

127. Dharan A, Opp S, Abdel-Rahim O, Keceli SK, Imam S, Diaz-Griffero F, et al. 2017. Bicaudal D2 facilitates the cytoplasmic trafficking and nuclear import of HIV-1 genomes during infection. Proc Natl Acad Sci U S A 114:E10707–E10716. https://doi.org/10.1073/pnas.1712033114 PMID: 29180435

128. O'Brien M, Manches O, Wilen C, Gopal R, Huq R, Wu V, et al. 2016. CD4 Receptor is a Key Determinant of Divergent HIV-1 Sensing by Plasmacytoid Dendritic Cells. PLoS Pathog 12:e1005553. https://doi.org/10.1371/journal.ppat.1005553 PMID: 27082754

129. Oguin TH 3rd, Sharma S, Stuart AD, Duan S, Scott SA, Jones CK, et al. 2014. Phospholipase D facilitates efficient entry of influenza virus, allowing escape from innate immune inhibition. J Biol Chem 289:25405–25417. https://doi.org/10.1074/jbc.M114.558817 PMID: 25065577

130. Nonnenmacher ME, Cintrat JC, Gillet D, Weber T. 2015. Syntaxin 5-dependent retrograde transport to the trans-Golgi network is required for adeno-associated virus transduction. J Virol 89:1673–1687. https://doi.org/10.1128/JVI.02520-14 PMID: 25410859

131. Chen YJ, Liu X, Tsai B. 2019. SV40 Hijacks Cellular Transport, Membrane Penetration, and Disassembly Machineries to Promote Infection. Viruses 11.

132. Mbianda C, El-Meanawy A, Sorokin A. 2015. Mechanisms of BK virus infection of renal cells and therapeutic implications. J Clin Virol 71:59–62. https://doi.org/10.1016/j.jcv.2015.08.003 PMID: 26295751

133. Schelhaas M, Malmstrom J, Pelkmans L, Haugstetter J, Ellgaard L, Grunewald K, et al. 2007. Simian Virus 40 depends on ER protein folding and quality control factors for entry into host cells. Cell 131:516–529. https://doi.org/10.1016/j.cell.2007.09.038 PMID: 17981119

134. Bennett SM, Jiang M, Imperiale MJ. 2013. Role of cell-type-specific endoplasmic reticulum-associated degradation in polyomavirus trafficking. J Virol 87:8843–8852. https://doi.org/10.1128/JVI.00664-13 PMID: 23740996

135. Caller LG, Davies CTR, Antrobus R, Lehner PJ, Weekes MP, Crump CM. 2019. Temporal Proteomic Analysis of BK Polyomavirus Infection Reveals Virus-Induced G2 Arrest and Highly Effective Evasion of Innate Immune Sensing. J Virol 93. https://doi.org/10.1128/JVI.00595-19 PMID: 31142673

136. Van Doorslaer K, Chen D, Chapman S, Khan J, McBride AA. 2017. Persistence of an Oncogenic Papillomavirus Genome Requires cis Elements from the Viral Transcriptional Enhancer. mBio 8. https://doi.org/10.1128/mBio.01758-17 PMID: 29162712

137. Van Doorslaer K, Porter S, McKinney C, Stepp WH, McBride AA. 2016. Novel recombinant papillomavirus genomes expressing selectable genes. Sci Rep 6:37782. https://doi.org/10.1038/srep37782 PMID: 27892937

138. Chapman S, McDermott DH, Shen K, Jang MK, McBride AA. 2014. The effect of Rho kinase inhibition on long-term keratinocyte proliferation is rapid and conditional. Stem Cell Res Ther 5:60. https://doi.org/10.1186/scrt449 PMID: 24774536

139. Campos SK, Ozbun MA. 2009. Two highly conserved cysteine residues in HPV16 L2 form an intramolecular disulfide bond and are critical for infectivity in human keratinocytes. PLoS One 4:e4463. https://doi.org/10.1371/journal.pone.0004463 PMID: 19214230

140. Pyeon D, Lambert PF, Ahlquist P. 2005. Production of infectious human papillomavirus independently of viral replication and epithelial cell differentiation. Proc Natl Acad Sci U S A 102:9311–9316. https://doi.org/10.1073/pnas.0504020102 PMID: 15958530

141. Christensen ND, Dillner J, Eklund C, Carter JJ, Wipf GC, Reed CA, et al. 1996. Surface conformational and linear epitopes on HPV-16 and HPV-18 L1 virus-like particles as defined by monoclonal antibodies. Virology 223:174–184. https://doi.org/10.1006/viro.1996.0466 PMID: 8806551

142. Kim D, Langmead B, Salzberg SL. 2015. HISAT: a fast spliced aligner with low memory requirements. Nat Methods 12:357–360. https://doi.org/10.1038/nmeth.3317 PMID: 25751142

143. Liao Y, Smyth GK, Shi W. 2014. featureCounts: an efficient general purpose program for assigning sequence reads to genomic features. Bioinformatics 30:923–930. https://doi.org/10.1093/bioinformatics/btt656 PMID: 24227677

144. Love MI, Huber W, Anders S. 2014. Moderated estimation of fold change and dispersion for RNA-seq data with DESeq2. Genome Biol 15:550. https://doi.org/10.1186/s13059-014-0550-8 PMID: 25516281

145. R Core Team. 2020. R: A language and environment for statistical computing, on R Foundation for Statistical Computing, Vienna, Austria. https://www.R-project.org/.

146. RStudio Team. 2020. RStudio: Integrated Development for R, *on* RStudio, Inc., Boston, MA. http://www.rstudio.com/.

147. Raudvere U, Kolberg L, Kuzmin I, Arak T, Adler P, Peterson H, et al. 2019. g:Profiler: a web server for functional enrichment analysis and conversions of gene lists (2019 update). Nucleic Acids Res 47: W191–W198. https://doi.org/10.1093/nar/gkz369 PMID: 31066453

148. Kolde R. 2019. pheatmap: Pretty Heatmaps. https://cran.r-project.org/package=pheatmap

149. Blighe K. 2019. EnhancedVolcano: Publication-ready volcano plots with enhanced colouring and labeling. https://github.com/kevinblighe/EnhancedVolcano